Computer Simulation of Pressure Fields Generated by Acoustic Lens Beamformers

by

Kevin Fink

A thesis submitted in partial fulfillment
of the requirements for the degree of

Master of Science
in Electrical Engineering

University of Washington

1994

Approved by _____
(Chairperson of Supervisory Committee)

Program Authorized
to Offer Degree _____

Date _____

In presenting this thesis in partial fulfillment of the requirements for a Master's degree at the University of Washington, I agree that the Library shall make its copies freely available for inspection. I further agree that extensive copying of this thesis is allowable only for scholarly purposes, consistent with "fair use" as prescribed in the U.S. Copyright Law. Any other reproduction for any purposes or by any means shall not be allowed without my written permission.

Signature _____

Date _____

University of Washington

Abstract

Computer Simulation of Pressure Fields Generated by Acoustic Lens Beamformers

by Kevin Fink

Chairperson of the Supervisory Committee:

Professor Ed Belcher
Department of Electrical Engineering

The Acoustic Lens Simulation Software Package (ALSSP) was developed to analyze acoustic lens systems; specifically, to predict the performance of a system design before fabrication. Given a design, the simulation calculates the complex pressure field behind the lens as a function of temperature, frequency, source position, and the transducer element. It also calculates beam patterns and finds focal points. The simulation uses a hybrid geometric/wave acoustic model which utilizes geometrical acoustics within the lens system and wave acoustics in image space. Ray tracing in two or three dimensions is used to implement the geometrical acoustics section, while numerical integration of the Kirchhoff integral or a complex summation of virtual sources may be used in the wave acoustics section. Lens systems may have any number of components placed arbitrarily in three dimensional space. The components are specified by their interfaces, which may be planar, spherical, or aspherical (including paraboloids, hyperboloids, and ellipsoids), and the parameters of the material between the interfaces. Several sound sources and transducer element types are available. The primary contribution of ALSSP is its applicability to a wide variety of acoustic lens systems and its inclusion of environmental effects.

Table of Contents

List of Figures

List of Tables

ACKNOWLEDGEMENTS

I would like to express my sincere appreciation to Kevin Williams at the Applied Physics Laboratory, who provided the basis for this work as well as numerous helpful suggestions and explanations of the underlying physics. I would also like to thank Mr. Donald Folds of ARINC Corporation for his method of calculating the pressure fields and his help in verifying results. Most of all, I would like to thank Dr. Ed Belcher for his support and guidance, for his enthusiasm about life, and for his confidence in me. Finally, I would like to thank my parents for all the work they did getting me to this point and for their continual love and support, as well as for proofreading this thesis.

INTRODUCTION

Acoustic beamforming modifies the propagation of sound by introducing spatially dependent delays into a wavefront. This focuses incoming sound from a single source or direction into a small volume of space so that it can be detected by a single transducer. Acoustic beamforming can be implemented using electronic circuitry or an acoustic lens.

Electronic beamforming uses a transducer array coupled with analog or digital signal processing circuitry to form beams. Sum and delay beamforming and narrowband phase-shift beamforming are two widely used algorithms implemented by the circuitry. The amount of signal processing circuitry and required power both increase with the number of transducers. This becomes a critical problem when large arrays are needed, especially for portable systems such as diver-held or autonomous underwater vehicle sonar systems.

Acoustic lenses implement beamforming with minimal associated circuitry. An acoustic lens focuses sound in much the same way that an optical lens focuses light. Snell's law describes the refraction of sound as it passes through an interface between two materials of differing sound speed. An acoustic lens provides the appropriate material thicknesses that focus a parallel wavefront of sound to a single focal point.

Acoustic lenses can be differentiated into two types: thick and thin. The focal point of a thick lens lies within the lens material, whereas the focal point of a thin lens is outside of the lens material (Figure 1). Either type may be a compound lens, with multiple layers of materials of differing refractive indices. Compound lens systems can be designed to optimally focus sound from several source directions or to reduce the sensitivity of the system to varying ambient temperatures.

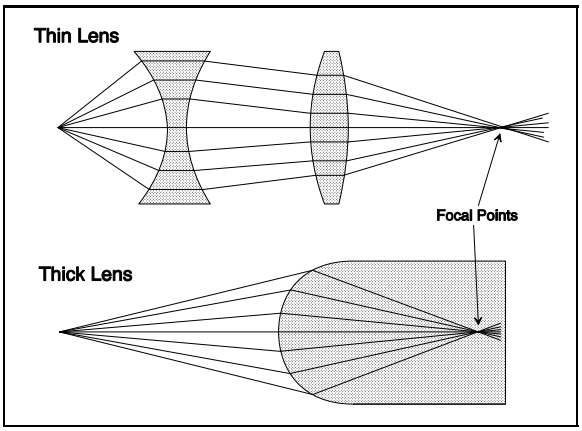

Figure 1 - Acoustic Lense Types

Purpose of Work

While acoustic lenses have been successfully designed and built, the only way to verify a system design has been to test a working model, an expensive and time-consuming process. The Acoustic Lens Simulation Software Package (ALSSP) was developed to predict the performance of an acoustic lens before fabrication. Given a design, the simulation determines the beam pattern as a function of temperature, frequency, source position, and the transducer element. ALSSP is currently being used as a check against another analysis package on the design of two thin lens systems; a 3 MHz imaging sonar and a dual-frequency detection sonar.

Relationship of Current Effort to Previous Work

The earliest generation of acoustic lens design analysis methods used only geometrical acoustics to characterize a lens system. While providing focal points, measures of spherical aberration, and other parameters needed for design, geometrical acoustics lacks diffraction effects and thus doesn't predict beam widths or sidelobe heights. In order to predict these parameters, acoustic lens simulations must include wave acoustics. The implementation of wave acoustics requires solving the differential wave equation(s) for the system, which can be rewritten as the Kirchhoff integral, which does not have a closed-form solution for any non-trivial lens systems.

Two methods of implementing wave acoustics have been proposed. The first is to numerically integrate the Kirchhoff integral, thereby approximating the solution. The second method is to use the underlying principle behind the Kirchhoff integral, the Huygens-Fresnel theory. The resulting implementation involves summing the contributions of virtual point sources to find the solution at a specific point in space.

Cornelius & Williams[1] examined the pressure field formed behind a hemispherical thick acoustic lens. Their method incorporates concepts from both

1 T.A. Cornelius and K.L. Williams, Note on the Calculation of the Spherically Aberrated Field of an Acoustic Lens, Technical Memorandum APL-UW TM 7-92, Applied Physics Laboratory, University of Washington, 1992.

geometrical and wave acoustics to calculate the pressure field behind the lens. In order to calculate the complex pressure field, the Kirchhoff integral is numerically integrated using pressures generated by ray tracing for boundary values.

Mr. Donald Folds of ARINC Corporation also developed a software simulator for acoustic lenses[2]. It uses a similar hybrid geometric/wave approach, but employs a different method to calculate the pressure field. Rather than integrating the Kirchhoff integral, it directly calculates the pressure field by summing the contributions of virtual point sources on the final lens surface[3]. Direct summation replaces numerical integration and the complex pressures on the final lens surface act as boundary values. The magnitude and phase of the virtual point sources are generated by ray tracing, as in the integration scheme.

Other efforts have been made to simulate the beam patterns of specific acoustic lenses using similar methods. Folds simulated a variety of lens systems, including a cylindrical liquid-filled (thick) lens[4,5], a four-element thin lens[6], and a variety of cylindrical single and multi-element thin lenses[7]. Beaver, Dameron, and Macovski

2 Personal Communication. 1993.

3 D.L. Folds, "Status of Ultrasonic Lens Development," Underwater Acoustics and Signal Processing, pp. 263-279, D. Reidel Publishing Company, 1981.

4 D.L. Folds, "Focusing Properties of a Cylindrical Liquid-Filled Compound Acoustic Lens," The Journal of the Acoustical Society of America, Vol. 49 No. 5 (Part 2), 1971.

5 D.L. Folds and D.H. Brown, "Focusing Properties of Cylindrical Liquid-Filled Acoustic Lenses with Large Diameter-to-Wavelength Ratios," The Journal of the Acoustical Society of America, Vol. 43 No. 3, 1968.

6 D.L. Folds, "Focusing properties of a solid four-element ultrasonic lens," Journal of the Acoustical Society of America, Vol. 58 No. 1, July 1975. pg. 74.

7 D.L. Folds, "Focusing properties of solid ultrasonic cylindrical lenses," The Journal of the Acoustical Society of America, Vol 53 No 3, 1973. pp 830-831.

simulated a single-element thin acoustic lens operating at 2.25 MHz[8]. Oh and Park simulated the beam pattern of a lens system that included both a thin lens mounted on the transducer element and a reflector[9,10].

Other methods have also been used to find sound pressure levels near a lens. Makarchenko, Rozhin, and Tonakanov investigated a liquid spherical lens using the exact solution of the Kirchhoff integral[11]. Penttinen and Luukkala transformed a single-surface lens into a curved transducer having the same focusing properties as the lens. They then used the rapid impulse method to compute the pressure distribution.[12]

ALSSP includes both the numerical integration method used by Cornelius and Williams and the summation method used by Folds and others. The integration method assumes that the lens system is radially symmetric and exploits that symmetry in order to provide increased execution speeds. However, this restricts its applications to radially symmetric lens systems with on-axis sources. The summation method does not make any assumptions about the lens system or source location, so is more universally applicable. The ray tracing can be confined to two dimensions when desired in order to speed analysis, but is performed in three dimensions by default.

8 W.L. Beaver, D.H. Dameron, and A. Macovski, "Ultrasonic Imaging with an Acoustic Lens," IEEE Transactions on Sonics and Ultrasonics, Vol. SU-24, No. 4, July 1977.

9 J.T. Oh and S.B. Park, "Optimal Design of a Transmit/Receive System with a Reflector and a Transducer Lens for Long-Range Underwater Acoustic Imaging," IEEE 1991 Ultrasonics Symposium Proceedings, Vol 2, pp. 949-52. 1991.

10 J.T. Oh and S.B. Park, "Iterative design of a lensed transducer-reflector system for underwater acoustic imaging," The Journal of the Acoustical Society of America, Vol. 93, No. 2, pp. 1166-1174. February 1993.

11 N.N. Makarchenko, F.V. Rozhin, and O.S. Tonakanov, "On Choosing the Optimal Parameters of a Spherical Lens," Vestnik Moskovskogo Universiteta, Seriya 3 (Fizika Astronomiya). Vol.44 No. 5, pp. 32-6. 1989.

12 A. Penttinen and M. Luukkala, "Sound pressure near the focal area of an ultrasonic lens," Journal of Physics D: Applied Physics, Vol. 9, pp. 1927-36. 1976.

Due to the decreased number of intermediary steps required, the summation method is also much quicker than the numerical integration method.

The primary contribution of this software set is its generality. It can analyze any of the lens systems discussed above (with the exception of the reflector system analyzed by Oh and Park) and can also show the effects of varying system environment parameters such as water temperature, salinity, and frequency of operation.

Analysis Model

The propagation of sound through an acoustic lens can be modeled using either geometrical acoustics, wave acoustics, or a combination of both. The geometrical model works well within the lens system, but breaks down near the focal points. Wave acoustics describes sound propagation more accurately in the focal regions, but is mathematically untenable within the lens. The simulation uses a hybrid model in which geometrical acoustics is used within the lens interfaces, and wave acoustics is used in the image space (Figure 2).

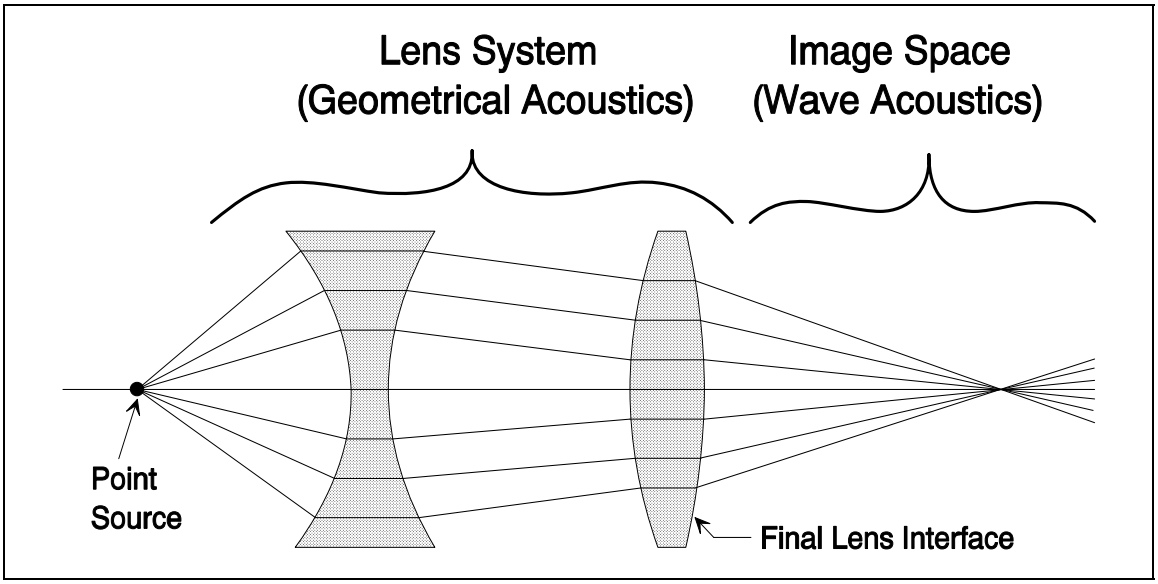

Figure 2 - Lens System Overview: Hybrid Approach

Acoustic lens design uses the same methods as optical lens design. These methods rely on ray tracing, which is a geometrical concept providing an

approximation to the true behavior of the lens. The accuracy of the approximation depends on the size of the lens system with respect to the wavelength of light or sound passing through it. For most optical systems, this ratio is very large, providing a good approximation. However, the wavelength of sound in most acoustic applications is significant with respect to realistic lens sizes, and thus the geometrical approximations do not work as well.

Wave acoustics theory provides a more accurate description of the behavior of sound, but is more complicated. The integral equations that describe sound propagation across interfaces in wave acoustics are often difficult or impossible to solve in closed form, and require substantial processing time to solve numerically.

The simulation implemented in ALSSP uses geometrical acoustics within the lens system and wave acoustics in the focal region. The transformation from geometrical to wave acoustics occurs at a point where both are feasible and accurate; the final lens interface. Geometrical acoustics, realized by ray-tracing, calculates the complex pressures on the final lens interface. Wave acoustics uses those pressures as boundary values in order to solve the Kirchhoff integral, which gives the pressure at points in the focal region.

The ray-tracing code included in ALSSP neglects the reflected component of rays. It has been experimentally determined that shell thicknesses of odd quarter wavelengths attenuate the sound pressure more than shell thicknesses of even quarter wavelengths[13]. This is probably an effect of interference due to reflection within the shell, and thus is not modelled by this simulation.

13 E. O. Belcher, C. May, and E. Pence, "Active Acoustic Lens with Large Field of View, Final Report," Technical Report APL-UW TR8918, Applied Physics Laboratory, University of Washington. June 1989. pp. 5-7.

Chapter 1: GEOMETRICAL ACOUSTICS

Sound, like light, may be described as rays or waves. In many cases, the laws governing sound's behavior can be described geometrically using ray theory. Geometrical acoustics predicts the refraction of sound at interfaces between materials of differing refractive indices. Tracing rays through a lens system yields approximate focal positions, magnification factors, and measures of spherical aberration.

However, geometrical acoustics breaks down in certain circumstances. At the focal point of a lens system, where many rays cross, geometrical acoustics predicts infinite sound pressures. On the other hand, it predicts zero pressure levels outside of the region of the lens system that contains rays. In reality, the pressure levels follow a somewhat smooth continuum, large but finite at the focal point, and small but non-zero outside the ray-containing region of the lens system.

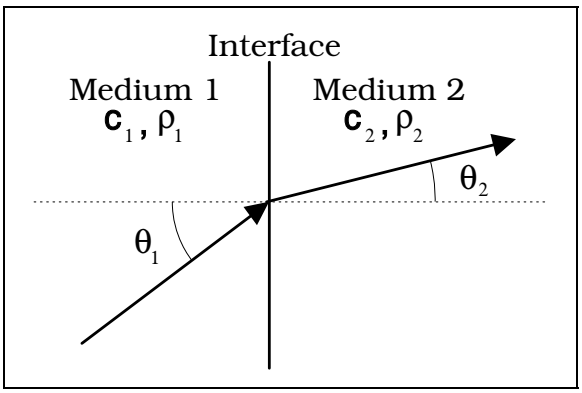

Figure 3 - Ray Tracing Terms

θ_1 is the angle of incidence,

θ_2 is the angle of refraction,

c_1 is the speed of sound in medium 1,

c_2 is the speed of sound in medium 2,

ρ_1 is the density of medium 1, and

ρ_2 is the density of medium 2.

In the ray tracing portion of the simulation, the initial magnitude of each ray is set to 1. Snell's Law is used to calculate the path of each ray as it passes through each interface:

$$\frac{\sin\theta_1}{\sin\theta_2} = \frac{c_1}{c_2}$$

The software also takes into account the sound attenuation due to each material and the transmission coefficient at each interface. In each section of the lens the sound attenuation, in dB/cm, is multiplied by the calculated physical path length to

find the attenuation. The total attenuation for each ray is the sum of the attenuation in each section of the lens.

The transmission coefficient depends on the angle of incidence at each interface and the densities and sound speeds of the materials at each interface. The equation is the solution of the wave equation for a parallel wavefront impacting a flat surface, thus it assumes that the curvature of each interface is small compared to the wavelength of sound. In terms of the parameters described in Figure 3, the transmission coefficient from one material to the next is

$$T_{12} = \frac{2\rho_2 c_2 \cos\theta_1}{\rho_2 c_2 \cos\theta_1 + \rho_1 c_1 \cos\theta_2}$$

The phase of each ray is the total acoustic path length of the route that it follows through the lens system minus the shortest acoustic path length for any ray. Thus all the ray phases are greater than or equal to zero, with zero phase corresponding to the shortest acoustic path length. The acoustic path length in each lens section is $\frac{2\pi fl}{c}$, where f is the frequency of the sound, l is the physical path length in the material, and c is the speed of sound in the material.

Once a ray trace has been made, an approximation of the pressure field along a given line can be found by calculating the density of rays crossing the line as a function of position along the line. In addition, the focal point can be approximated by finding the point in space that has the highest density of rays. As discussed before, however, this method predicts infinite intensity at the focal point and zero intensity outside of the ray-containing region of image space.

In order to determine whether or not an acoustic lens design will meet the design requirements, it is necessary to characterize it with more detail than geometrical acoustics permits. Two measurements of the beam pattern of a lens system that are particularly important are the beam width and the sidelobe heights. Geometrical acoustics predicts nothing about these parameters, but they can be found using wave theory.

Chapter 2: WAVE ACOUSTICS

The disparities between the predictions of geometrical acoustics and reality can be explained by taking into account the wave nature of sound. In addition to the lens interfaces refracting the sound, the edges of the lens diffract the sound, producing effects that can not be described by ray theory. This is especially apparent in acoustics, because the ratio of wavelength to lens dimension is much greater in acoustic applications than optical applications.

The Huygens-Fresnel principle describes sound as spherical waves emanating from a source[14] (Figure 4). Each point on the wavefront is considered a source of secondary spherical wavelets with appropriate amplitude and phase. The amplitude of the pressure field in front of the wavefront is the superposition of these wavelets, taking into account their relative amplitudes and phases. The amplitude of each wavelet is largest in the direction of the original wavefront's propagation and zero in the opposite direction. The relative amplitude of each portion of the wavelet is described by the obliquity factor $K(\theta)=\frac{\cos\theta + 1}{2}$, where θ is the angle between the wavelet's direction and the original wavefront's propagation direction. Kirchhoff diffraction theory puts the Huygens-Fresnel principle into mathematical form by solving the scalar differential wave equation.

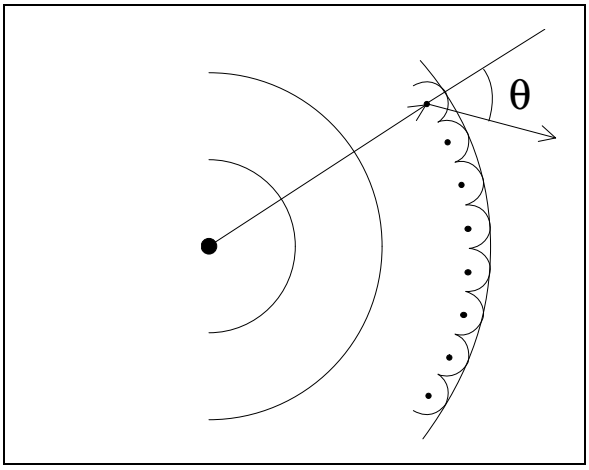

Figure 4 - The Huygens-Fresnel Principle

There are several ways to calculate the pressure field based on the Huygens-Fresnel principle/Kirchhoff's diffraction theory. Kirchhoff's diffraction theory expresses the complex pressure at a point in image space by the two-dimensional

14 E. Hecht, Optics, Addison-Wesley Publishing Company, 2nd Ed., 1990. pg. 434.

Kirchhoff integral. This can be solved numerically at each desired point in the pressure field to find the complex pressure. The Huygens-Fresnel principle can also be used more directly to find the pressure at a point by summing the contributions of virtual point sources arrayed on the final surface of the lens system. This requires expressing the principle mathematically as a summation rather than an integration, but approaches the Kirchhoff integral in the limit.

2.1 Kirchhoff Integration Method

Cornelius & Williams evaluated the Kirchhoff integral at points in the pressure field in order to find the complex pressure. The complex pressure field on the exit

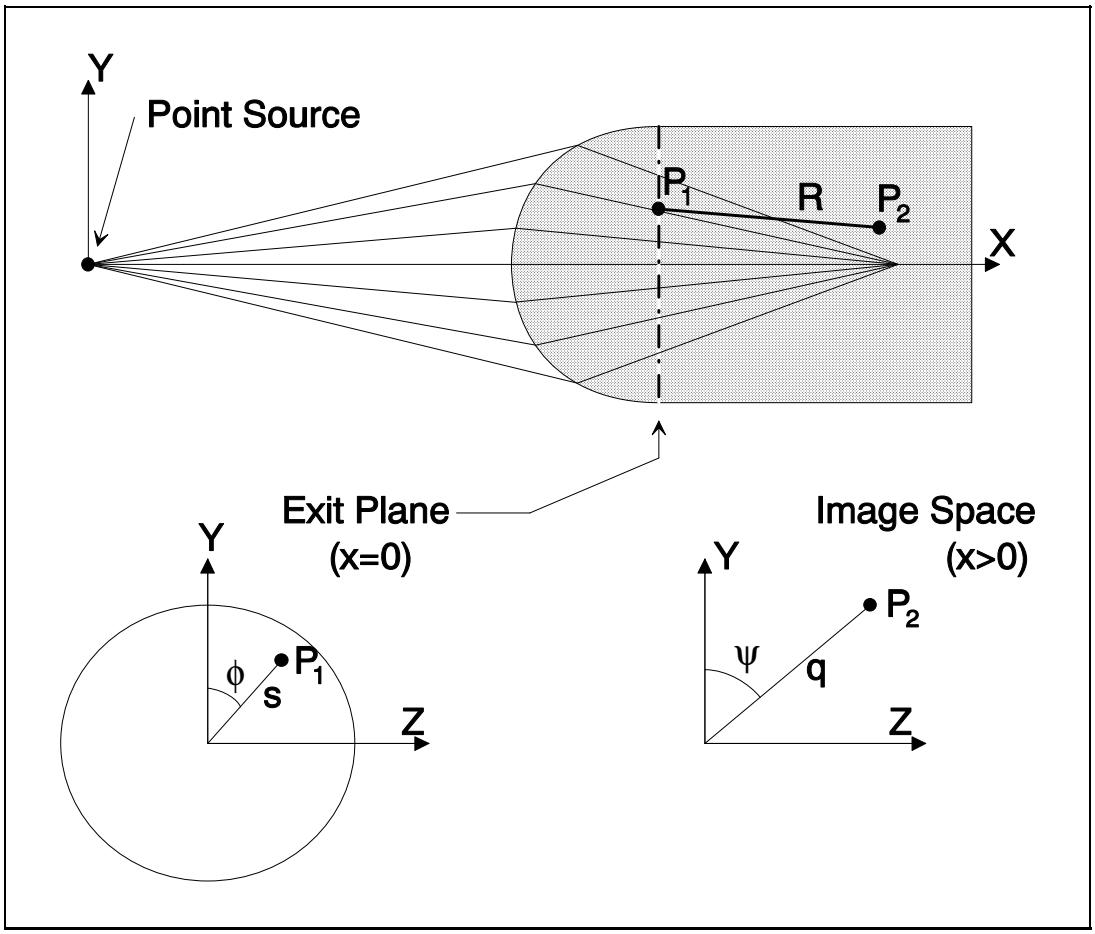

Figure 5 - Lens Geometry for Integration Method

plane of the lens is used as the boundary conditions that are needed to solve the Kirchhoff integral. The exit plane of the lens is a plane normal to the principal (x) axis of the lens system, placed immediately after the final lens surface (see Figure 5). A collection of rays are traced through the lens, keeping track of the amplitude and phase of each ray. The complex pressure on the exit plane is the amplitude and phase of each ray where it intersects the exit plane. The magnitude is also scaled by the density of rays intersecting the exit plane near each point.

Because the rays will pass through a smaller section of the plane if the exit plane is placed farther from the final lens surface, more diffraction effects will be lost, resulting in decreased accuracy. Thus the exit plane is placed as close as possible to the final lens surface.

In terms of the coordinate system shown in Figure 5, the Kirchhoff integral is written as[15]

$$P(x,\psi,q) = -\frac{1}{2\pi}\int\int P(x=0,\phi,s)\frac{\partial}{\partial x}\left[\frac{e^{ikR(\phi,s,x,\psi,q)}}{R(\phi,s,x,\psi,q)}\right] s\,ds\,d\phi \qquad (1)$$

where

$P(x,\psi,q)$ is the complex pressure at point P_2 in image space,

$P(x=0,\phi,s)$ is the complex pressure at point P_1 on the exit plane,

$k=(2\pi)/\lambda=(2\pi f)/c$ is the wave number, with λ the wavelength, f the frequency, and c the speed of sound in the medium,

R is the distance between the point $P_1=(x=0,\phi,s)$ on the exit plane and the point $P_2=(x,\psi,q)$ in image space, and

15 T.A. Cornelius and K.L. Williams, Note on the Calculation of the Spherically Aberrated Field of an Acoustic Lens, Technical Memorandum APL-UW TM 7-92, Applied Physics Laboratory, University of Washington, 1992. pg. 21.
For a more detailed derivation, see E. Hecht, Optics, Addison-Wesley Publishing Company, 2nd Ed., 1990. pg. 459-463.

e^{ikR}/R is the point-source Green's function, which describes the point source as a disturbance of the pressure field.

Expanding the partial derivative, the integral becomes

$$P(x,\psi,q) = -\frac{1}{2\pi}\int\int P(x=0,\phi,s)\frac{(ik-1/R)xe^{ikR(\phi,s,x,\psi,q)}}{R^2(\phi,s,x,\psi,q)}sdsd\phi \tag{2}$$

For **R** large with respect to the wavelength of sound, this can be approximated by

$$P(x,\psi,q) = -\frac{ikx}{2\pi}\int\int P(x=0,\psi,s)\frac{e^{ikR(\phi,s,x,\psi,q)}}{R^2(\phi,s,x,\psi,q)}sdsd\phi \tag{3}$$

Cornelius & Williams analyzed an axially symmetric lens. Therefore, ψ is set to 0, so $q=y$ and the pressure on the exit plane $P(x=0,\psi,s)$ becomes a function of s only, simplifying the equation to

$$P(x,y) = -\frac{ik_t x}{2\pi}\int\int P(s)\frac{e^{ik_t R(\phi,s,x,y)}}{R^2(\phi,s,x,y)}sdsd\phi \tag{4}$$

In these equations, the obliquity factor is approximated by the $\frac{x}{R}$ term, which becomes $\cos\theta$ for a parallel wavefront (the incoming rays are parallel to the x-axis), which is approximately equal to $\frac{\cos\theta+1}{2}$ for small θ.

In order to numerically evaluate this integral, Cornelius & Williams used Simpson's Composite Integration Formula with a fixed order of 50 in each dimension. This is a conceptually simple approach, but it does not guarantee either convergence or efficiency. Numerical integration using Simpson's Formula of order 50 does not converge properly for some lens configurations but would converge at a much smaller

order (and thus more quickly) for others. Lack of convergence of the inner integral leads to a large error after performing the outer integral even if the outer integral converges, since its integrand is incorrect. Increasing the order to a larger number ensures convergence, but also dramatically increases the time required to compute the integral.

A second numerical integration algorithm was implemented in order to improve the numerical integration in the simulation. The Romberg integration formula is an adaptive scheme that uses polynomial interpolation and successively decreasing step sizes to quickly evaluate the integral. The integration tolerances can be changed to balance accuracy against speed, and the integration only proceeds until convergence is reached, reducing the overall time required. This method results in faster evaluation of the integral in most cases, and provides more security in terms of convergence for all lens systems.

2.2 Summation Method

An alternate method[16] for finding the pressure field behind a lens simplifies the calculation by dispensing with the transformation from discrete to continuous representation and then from continuous back to discrete representation as is required for numerical integration. In the Kirchhoff integration method, the first step is discrete: a finite number of rays are traced through the lens system to the exit plane. Then a continuous function is synthesized from them to place within the integral. Finally, the integral is evaluated by approximating it numerically as a summation.

In the summation method, rays are traced from a source through the lens system, but terminate on the final lens surface rather than continuing to an exit plane. This eliminates the errors that arise from assuming no diffraction occurs between the final lens surface and the exit plane. Each point on the final lens surface where a ray hits is considered a point source as in Kirchhoff's diffraction theory. Rather than evaluating an integral for each position in the resulting pressure field, however, the

16 Mr. Don Folds, Personal Communication. 1993.

contribution of each point source, weighted according to the obliquity factor and its distance to the point of interest, is summed.

Referring to Figure 6, assume that **N** rays have been successfully traced through the system. Let **V[n]** denote the **(x,y,z)** coordinates of the point where ray **n** intersects the exit surface and **P[n]** represent the complex pressure of that virtual source. Further, let **D[n]** be a direction vector representing the ray's direction of travel at that point. The distance from each virtual source to the image point is

$$\boldsymbol{R}[n]=\sqrt{(x-V_x[n])^2+(y-V_y[n])^2+(z-V_z[n])^2}.$$

The direction vector from each virtual source to the image point is

$$D'[n]=\begin{bmatrix}x\\y\\z\end{bmatrix}-V[n]=\begin{bmatrix}x-V_x\\y-V_y\\z-V_z\end{bmatrix}$$

The obliquity angle is the angle between each ray's terminal direction of travel and the direction from the virtual source to the image point:

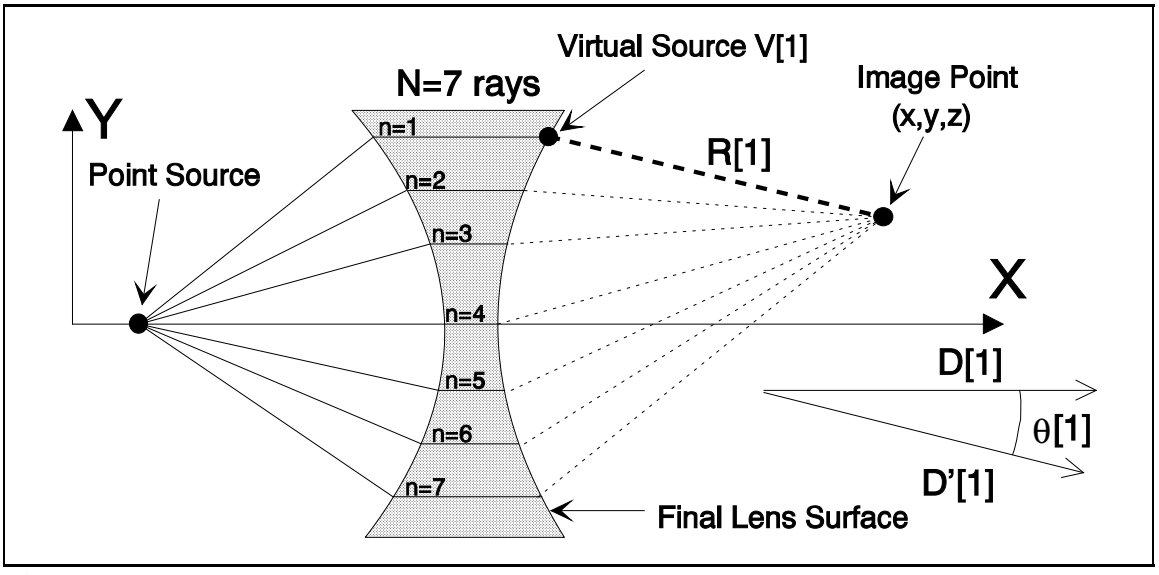

Figure 6 - Lens Geometry for Summation Method

$$\theta[n] = \langle D[n], D'[n] \rangle = D_x[n]D'_x[n] + D_y[n]D'_y[n] + D_z[n]D'_z[n]$$

The obliquity factor is:

$$O[n] = \frac{\cos\theta[n] + 1}{2}$$

The attenuation due to the absorption of the fluid between the exit surface and the retina is found by multiplying the fluid's attenuation coefficient, in dB/cm, by the distance from the virtual source to the image point, in cm, then converting from dB to magnitude:

$$A[n] = 10^{\frac{Attenuation\_Coefficient * R[n]}{20}}$$

The final factor is the point spread (or Green's) function for the virtual source:

$$S[n] = \frac{e^{ikR[n]}}{R[n]}$$

The complex pressure at any point in image space $P(x,y,z)$ will be the sum of the contributions of all the virtual sources, taking into account the relative magnitude and phase of each virtual source.

$$P(x,y,z) = \sum_{n=1}^{N} O[n]A[n]S[n]P[n]$$

Substituting in the previously described functions, the equation becomes:

$$P(x,y,z) = \sum_{n=1}^{N} \frac{\cos\theta[n] + 1}{2} 10^{\left(\frac{Attenuation\_Coefficient * R[n]}{20}\right)} \frac{e^{ikR[n]}}{R[n]} P[n] \qquad (5)$$

2.3 Comparison of Integration and Summation Methods

Equations (4) and (5) should be equivalent in the limit, but some differences are apparent. The summation method has an attenuation term, which was not included in the integration method. The obliquity factor in the summation method is approximated by the $\frac{x}{R}$ term, as discussed earlier. The boundary values $P(s)$ on the exit plane for the Kirchhoff integral are replaced by values $P[n]$ on the final lens surface for the summation method. The summation method does not have the $-i = e^{i(-\pi/2)}$ term and thus differs from the integration method by a $\pi/2$ phase shift. This is missing from the Huygens-Fresnel theory[17], but since only the relative phases between points in the pressure field are of interest, it is unnecessary to include it.

2.4 Spatial Aliasing

When using the summation method, convergence depends on the number of rays traced through the lens system. If an insufficient number of rays are traced, the beam patterns will be spatially aliased. Spatial aliasing is avoided in the integration schemes discussed above by checking that the integrand is sufficiently smooth before performing the integration. However, spatial aliasing is quite easy to detect in beam patterns due to its regularity, and can be avoided by choosing a sufficient number of rays.

A general rule of thumb is to choose the spacing of rays between $\lambda/10$ and $\lambda/2$[18]. For example, for a 900 kHz system with a 30 cm aperture, $\lambda/2$ corresponds to 373 rays. Figure 7 shows the generated beam pattern for an example system using 301 rays. In a beam pattern generated by tracing only 11 rays (Figure 8), aliasing is

17 E. Hecht, Optics, Addison-Wesley Publishing Company, 2nd Ed., 1990. pg. 462.

18 Mr. Don Folds, Personal Communication.

clearly visible. However, increasing the number of rays traced only to 31 moves the aliased mainlobe out to 6.73 cm (7.95°), reducing the effects of aliasing on the mainlobe and first two sidelobes to less than 1%. The rule of thumb described above, then, is very conservative. For this example, 31 rays, corresponding to about 5λ, is sufficient for good accuracy.

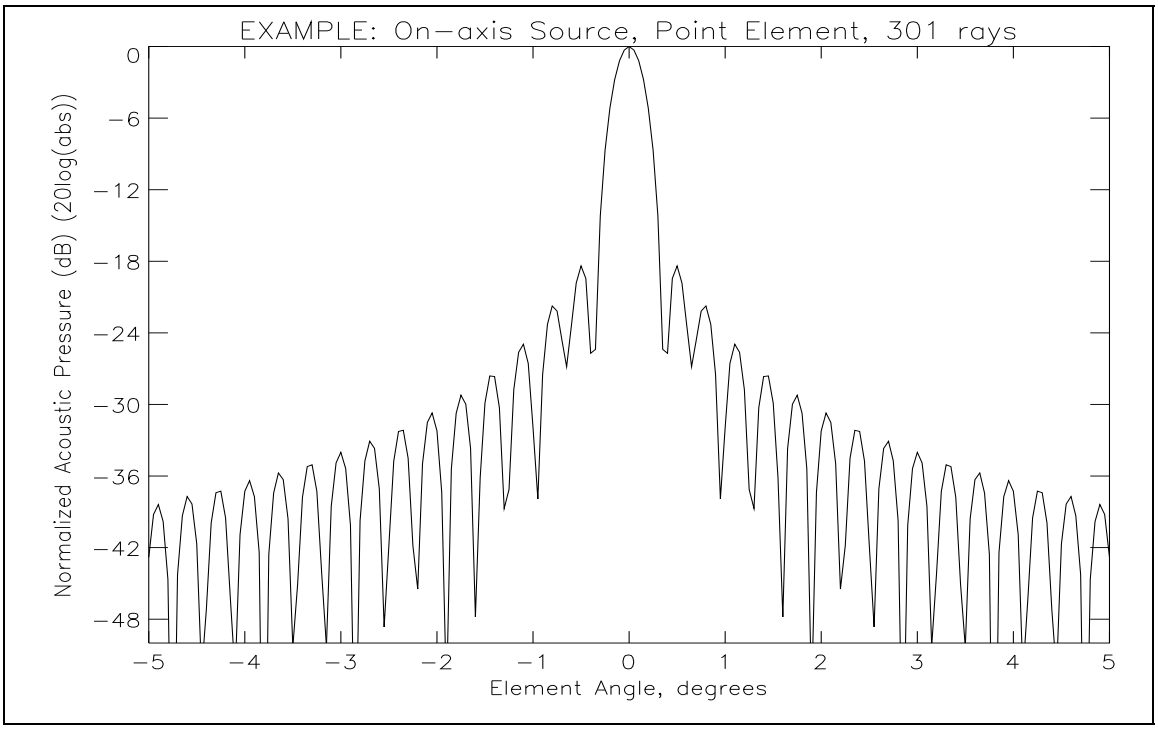

Figure 7 - Beam Pattern without Aliasing

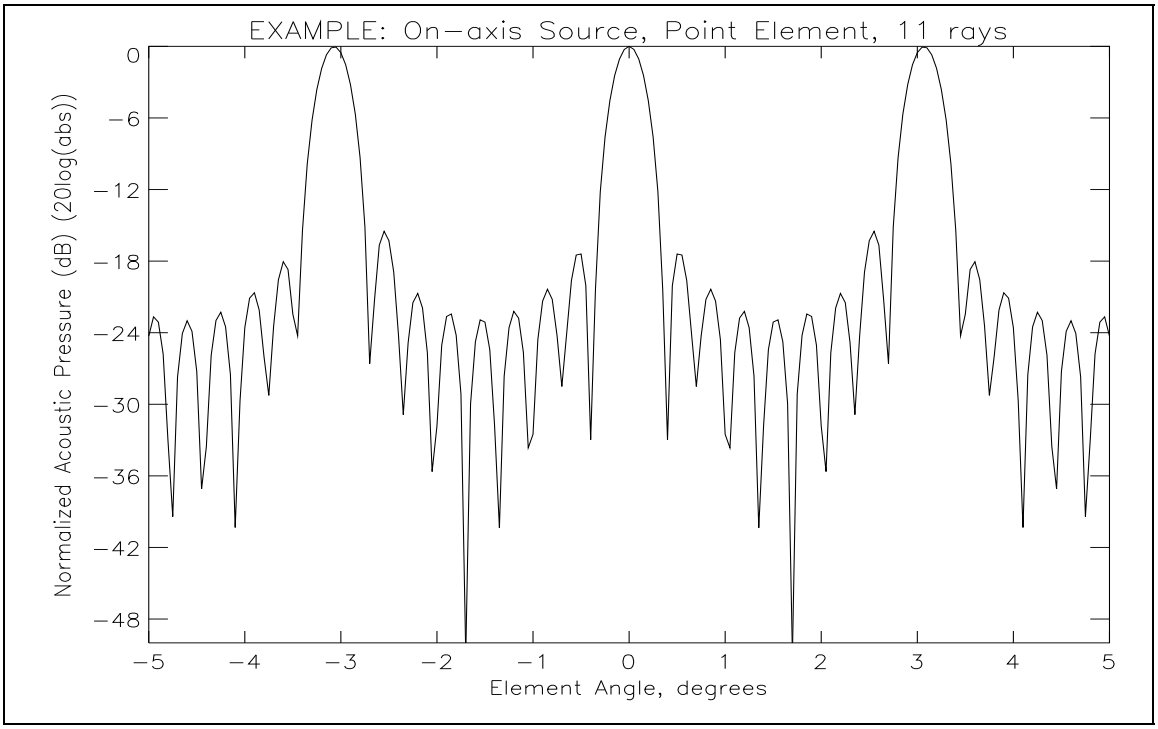

Figure 8 - Aliased Beam Pattern

Chapter 3: SOFTWARE SIMULATION

The Acoustic Lens Simulation Software Package (ALSSP) consists of 110 modules and 6500 lines of code. It runs under PV-WAVE, a programming language and environment by Precision Visuals[19]. It can be run either interactively on the PV-WAVE command line or non-interactively using batch files. The package takes into account the lens system's environment with ambient system parameters that include system temperature, salinity, depth, attenuation rate, sound speed, and frequency of operation. The ALSSP User's Guide contains a complete description of ALSSP, including all options and a complete representative example of a lens system analysis. A short functional description will be given here.

3.1 Capabilities

Lens systems may have any number of components placed arbitrarily in three dimensional space. The lens interfaces are planar, spherical, or aspherical, which includes hyperboloids, paraboloids, and ellipsoids. The density, sound attenuation rate, and sound speed of each lens material are also specified. Sound sources available are point sources, planar sources, and curved linear sources, while receive element types are point, rectangular, curved rectangular, and circular. The ray-tracing algorithms accommodate any number of rays, in either two or three dimensions. Plots of lens systems, with or without traced rays, may be viewed on the screen and/or printed.

ALSSP has the capability to calculate pressure fields, find focal points, and generate beam patterns. Pressure fields may be generated in several types of regions, including planar circles and rectangles, curved rectangles (i.e. cylinder sections), and rectangular volumes. Focal points may be found along lines or in rectangular regions of space. Beam patterns may be generated along lines, arcs, or piecewise-circular trajectories and include the effects of the receive element.

19 "PV-WAVE: Workstation Analysis and Visualization Environment," Precision Visuals, Inc., Boulder, CO. Copyright 1990.

3.2 Overview

The main program module of ALSSP is CALC_LENS. A block diagram is shown in Figure 9. Keyword parameters and a parameter file contain information on the lens system and type of calculation desired. The ray trace data is restored if previously saved, otherwise the ray trace is performed. The data can be saved at that point for later use. CALC_LENS then calls the appropriate module for the type of calculation desired.

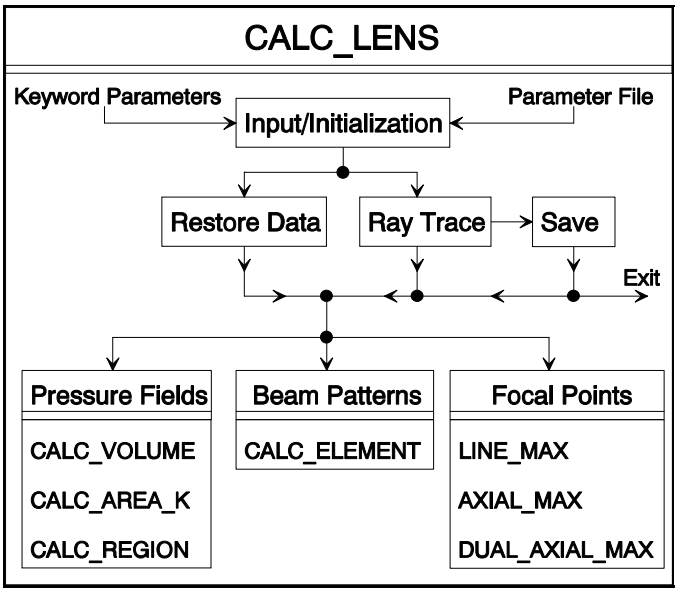

Figure 9 - CALC_LENS Block Diagram

3.3 System Environment

The lens system operates underwater. The system depth, water salinity, attenuation rate of sound in the water, density of the water, ambient water temperature, and system frequency must be specified. The speed of sound in the surrounding water can be specified in meters/second or the program will calculate it using the water depth, salinity, and temperature, using the formula[20]

20 C. S. Clay and H. Medwin, Acoustical Oceanography: Principles and Applications. John Wiley & Sons, 1977. pg. 3.

$$WaterSpeed = 1449.2 + 4.6T - 0.055T^2 + 0.00029T^3 + (1.34 - 0.010T)(Sal - 35) + 0.016Depth$$

where *WaterSpeed*=speed of sound in water, m/sec

T=water temperature, °C

Sal=water salinity, parts per thousand

Depth=water depth, meters

3.4 Control Parameters

The main program, CALC_LENS, takes a number of control parameters that specify how the results will be computed and stored, and how errors and other information will be logged. The program uses the summation method of calculating the pressure by default, but can also use the numerical integration method. The number of rays to trace must be specified. Ray tracing is done in three dimensions by default, but can be constrained to a plane if desired.

If the ray trace is to be displayed, the title, x and y ranges, axis titles, tick sizes, and plot color can be specified. The y-range can also be automatically set from the x-range to preserve a square aspect ratio (so that circles look like circles instead of ellipses). ALSSP can also display only a fraction of the rays that are actually traced in order to produce a less cluttered plot while preserving the accuracy of the calculations. Similarly, the ray plot can be restricted to the z=0 plane instead of projecting all rays into that plane.

A number of files may be specified in order to control how CALC_LENS computes and stores its results. The ray trace results can be saved independently of any other results and then restored later, so that calculations do not need to redo previously computed ray traces. In conjunction with this, the program can be told to compute ray trace results and save them but not to perform any additional calculations. The logging information that is normally displayed on the screen can be sent to a log file for later reference. The verbosity of the logging information can also be controlled. The file name that holds the calculated pressure field or beam pattern can be specified, although it defaults to the name of the input parameter file with '.out'

appended to the end. In addition, CALC_LENS can be commanded to enter view mode, in which the ray trace is displayed with 21x21 rays (or 21 rays for a 2D trace) and no results at all are saved or logged.

3.5 Sound Sources

The traced rays originate at a source, which can be a point, plane, or a curved or straight line. The usual type is a point source, in which all the rays emanate from a single point in space. In a planar source all incoming rays are parallel, which is equivalent to a point source at an infinite distance. The final type of source is a curved, linear source, defined by a set of equally spaced point sources arrayed along a curved line. The curvature of the line is set to 0 for a linear source.

3.6 Lenses

The lens system consists of any number of lenses, each specified by its interfaces. Interface types are planar, spherical, ellipsoidal, and aspherical. The aperture of each interface specifies the region through that rays may pass. Rays outside of the interface's aperture will be discarded. The material after each interface is specified by its sound speed, density, and sound attenuation rate.

A planar interface is specified only by its origin and aperture size, and thus is actually a circle in the yz-plane. Spherical and ellipsoidal interfaces are special cases of aspherical interfaces. Aspherical lens surfaces are spherical with an added shape factor that allows different conic classes.[21]

$$x = x_0 + \frac{cr^2}{1 + \sqrt{1 - sc^2 r^2}} \;;\; r^2 = (y - y_0)^2 + (z - z_0)^2$$

21 "Beam Three Optical Ray Tracer", Stellar Software, Berkeley, CA.

The curvature **c** is specified by 1/(radius of curvature at the center). The shape factor **s** can be:

Table 3.6 - Shape Factors	
s < 0	hyperboloid
s = 0	paraboloid
0 < **s** < 1	prolate ellipsoid
s = 1	sphere
s > 1	oblate ellipsoid

3.7 Calculation Types

ALSSP calculates complex pressure fields along a line, an arc, a calculated trajectory, or in a region of space. It also finds the focal point of a lens system along a line or in a plane. In addition, an element can be placed in the pressure field in all of the above calculations.

3.7.1 Beam Patterns

A beam pattern is a plot of magnitude vs. source angle: a plot of the response of a fixed transducer element to a moving point source. Calculating a beam pattern requires doing a separate ray trace and complex summation or integration for each source angle, which is computationally expensive. However, the beam pattern can be approximated by fixing the source and moving the element instead.

This approximation is very good in some cases, but falls short in others. The accuracy depends on the shape of the trajectory of focal points generated by moving the source. If the element is moved along this trajectory, the approximation will be very good. However, if the element is moved along a different trajectory, or the position along the trajectory is not correctly matched to the angles that generated it, the beam pattern will be inaccurate.

If the focal trajectory has only a small amount of curvature relative to the width of the desired beam pattern, a line cut through the pressure field may provide a

good approximation to the true focal trajectory. The approximation can be improved by finding an arc that follows the focal trajectory.

One method is to find the center of curvature and radius of an arc by finding the focal points due to two point sources, one on-axis and the other off-axis, and assuming that the center of curvature is on the principle axis of the lens system (Figure 10). The position of the center of curvature H" is called the secondary principal point. It is defined as the point that generates an arc radius forcing the arc angle to be equal to the source angle. With H" set, moving the transducer element Θ° is the same as moving the source Θ°. The radius of the arc is then set so the arc includes the focal point that generated it, which is assumed to be the center of the desired beam pattern.

$$H'' = x_1 - \frac{y_1}{\tan\theta}$$

$$r_0 = x_0 - H''$$

$$r_1 = \frac{y_1}{\sin\theta}$$

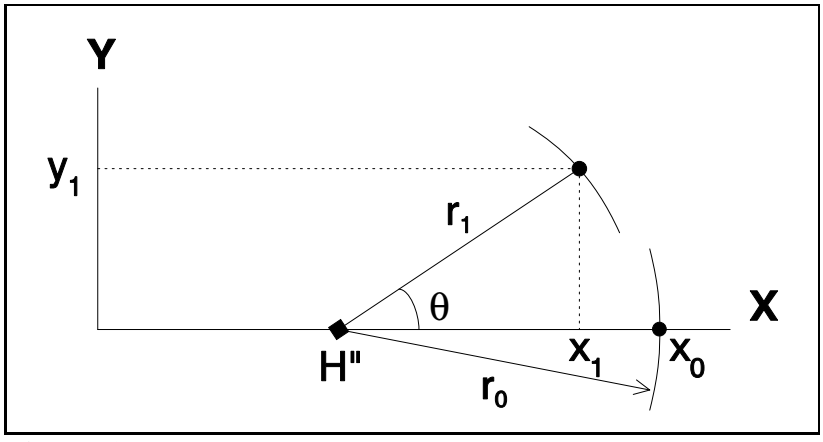

Figure 10 - Secondary Principal Point Determination

When the lens system has a focal trajectory with a more complicated curvature, moving the element along the focal trajectory will generate a better approximation of the beam pattern. In order to do this, the trajectory must be calculated by finding the focal points due to a number of source angles. Then the trajectory is approximated by a piecewise-circular function. (See the ALSSP User's Guide for more information.)

3.7.2 Pressure Fields

ALSSP will calculate pressures in a region of space. The region can be a rectangular volume, a planar rectangle or circle, or a curved rectangle (a section of a cylinder.)

A volume of space is specified by its origin (center), its size in three dimensions, and its sampling density in each dimension. Setting the size in one or more dimensions equal to zero selects a rectangular or linear region of space.

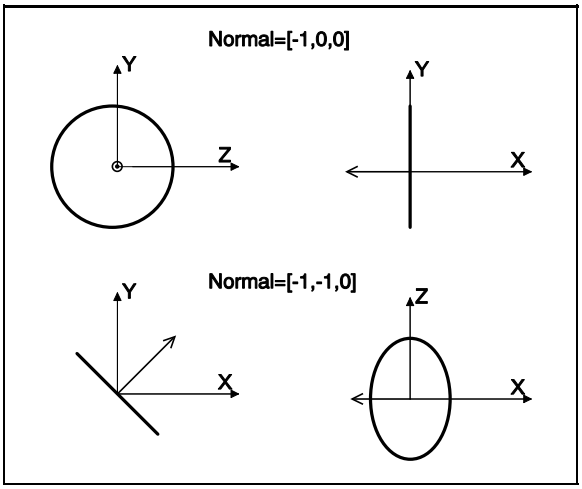

Figure 11 - Orientation Examples

Each of the other three regions are planar (or planar with a curve), and are specified by their origin, size, sampling density, and orientation. There are two ways to define a region's orientation in space. The simplest is by specifying the plane in which it lies: xy, xz, or yz. In these cases the sizes are specified directly in terms of the plane in which the region lies. If the xy plane is specified, then the first size refers to the x-direction and the second to the y-direction. Similarly, if the yz plane is specified, then the first refers to the y and the second to the z.

For more general orientations, the region's normal can be specified to define the direction in which the region faces. A normal of [0,-1,0] (parallel to the y-axis) would put the region in the x-z plane, and a normal of [-1,-1,0] would put the region parallel to the z-axis with its projection into the x-y plane a line with 45 degree angle (Figure 11).

Since the region is assumed to start in the y-z plane, care must be taken to specify the size correctly if another plane is desired. For example, for a rectangular region in the x-y plane with size in the x-direction of 10 cm and size in the y-direction of 5 cm, the orientation vector will be [0,0,1], but the size should be specified as 5,10 rather than 10,5, since the region will rotate around the y-axis, moving the second dimension from z to x but leaving the first as y.

A rectangle is specified by its origin (center), its size in two dimensions, the sampling density on its surface (in each dimension), and its orientation in space. A curved rectangle is a section of a cylinder wall, i.e. a rectangle that is curved in one dimension. A planar circle is specified identically to a rectangle, with the substitution of its radius for the rectangle's dimensions.

3.7.3 Focal Point Determination

The focal point of a lens system is defined as the point of maximum absolute pressure. The focal point can be found along a line or in a plane. The algorithm to find the focal point along a line is much faster than that for a plane, so should be used whenever possible.

In either case, a coarse search is done first over the search range in order to find a point near the global maximum, thus avoiding local maxima. Then the maximum is refined using a binary search until the accuracy condition is met. The accuracy is the distance between the maximum and the nearest two search points.

The planar algorithm finds the maximum parallel to the first axis at a fixed distance from the second axis (given by the initial guess.) Then it uses that point as the fixed distance from the first axis, and searches parallel to the second axis. This is repeated until the given accuracy is achieved. The algorithm is very slow to converge when searching along a ridge that lies at an angle to both axes, so when the maximum is known to lie along a certain line, it is much faster to search along that line. For example, in a single-element lens, the focal point will lie on the line extending from the source through the center of the lens.

3.8 Element Types

Four element types are available. The first, a point element, represents the actual pressure level at a point in space. The other three (rectangular, curved rectangular, and circular) represent the effect of placing a receive element of a certain size and shape at a point in the pressure field. Each element is specified by its center, with the additions of size in each dimension for the rectangular elements and the

radius of the circular element. The radius of curvature in each dimension must also be specified for the curved rectangular element, which is simply a smaller version of a curved rectangular region, described in section 3.7.2.

3.9 Element Orientation and Sampling Density

For any element except a point element, the element's orientation and sampling density must also be specified. The element can be oriented in one of two ways: so that it is always facing a specified direction, or so that it always faces a specific point, regardless of the element's position. In the first case, the orientation direction is specified identically to that of a rectangular pressure field (see section 3.7.2 and Figure 11).

Elements are approximated by summing the complex pressure field over the element's face, so the number of samples taken on the element's face must also be indicated. The accuracy of the approximation will increase with the number of samples, but the speed will decrease proportionately. Large elements require more samples than small elements. No general rule has been determined for choosing the number of samples on an element, but in practice it is easy to run trials with several sampling densities to determine when the response stops changing.

Chapter 4: UTILITY PROGRAMS

In addition to CALC_LENS, ALSSP contains a variety of utility programs designed to help in the design and analysis of lens systems. Complete descriptions of these are included in the ALLSP User's Guide. Included are programs to automate the creation of lens systems and set up the associated calculations, to plot pressure fields and beam patterns and annotate those plots, and to simplify the process of extracting data about lens systems from the stored results. Brief descriptions of the most important utility programs are given in Table 4.

Table 4 - ALSSP Utility Programs

ANNOTATE	Adds annotation (text) to a plot.
CONCAT_RESULTS	Assembles multiple source position results into a beam pattern. The resulting beam pattern is the response of a fixed transducer element to a moving point source.
FOCI_CIRC	Assembles pre-calculated focal points into a focal trajectory.
GENERATE_SYSTEM	Converts a BEAM THREE[22] OPTIC file to ALSSP parameter files for an array of source positions.
GET_LOG	Assembles the results of multiple focal point searches into a single array.
KLEGEND	Adds a legend to a plot.
KPLOT	Displays pressure fields and beam patterns. Also finds 3 dB points, sidelobe heights and positions, and maximum pressure points and values.
MAKE_BEAMS	Generates parameter files to calculate the response of an element at a single point to an array of source positions.
MAKE_BEAMS1	Generates parameter files to calculate the beam pattern for a system by moving the transducer element along the focal trajectory.
MAKE_BEAMS2	Creates parameter files to calculate beam patterns.
MAKE_LINE_MAX	Generates a parameter file to find the maximum response of an element along a line through a lens system's pressure field.
MAKE_MAX_REGION	Generates a parameter file to find the maximum response of an element within a region of space.
MAKE_VOLUME	Generates a parameter file to calculate the pressure field of a lens system within a region of space.
MAN	Gives a brief summary of an ALSSP routine.

22 "BEAM THREE OPTICAL RAY TRACER", Stellar Software, Berkeley, CA.

Chapter 5: CASE STUDIES

In order to verify the operation of the simulation, ALSSP's predictions will be compared to actual experimental data for three thick lens configurations. Next, ALSSP will be used to examine the changes in system performance due to changing various system parameters for an example thick lens system. Finally, a thin lens system will be analyzed to show how ALSSP is used in actual iterative lens design projects.

5.1 200 kHz Diver-Held Sonar Thick Lens Analysis

The first lens was designed for a diver-held sonar with 3° beams operating at 200 kHz[23]. It consists of a spherical rubber shell of inner radius 7.366 cm and outer

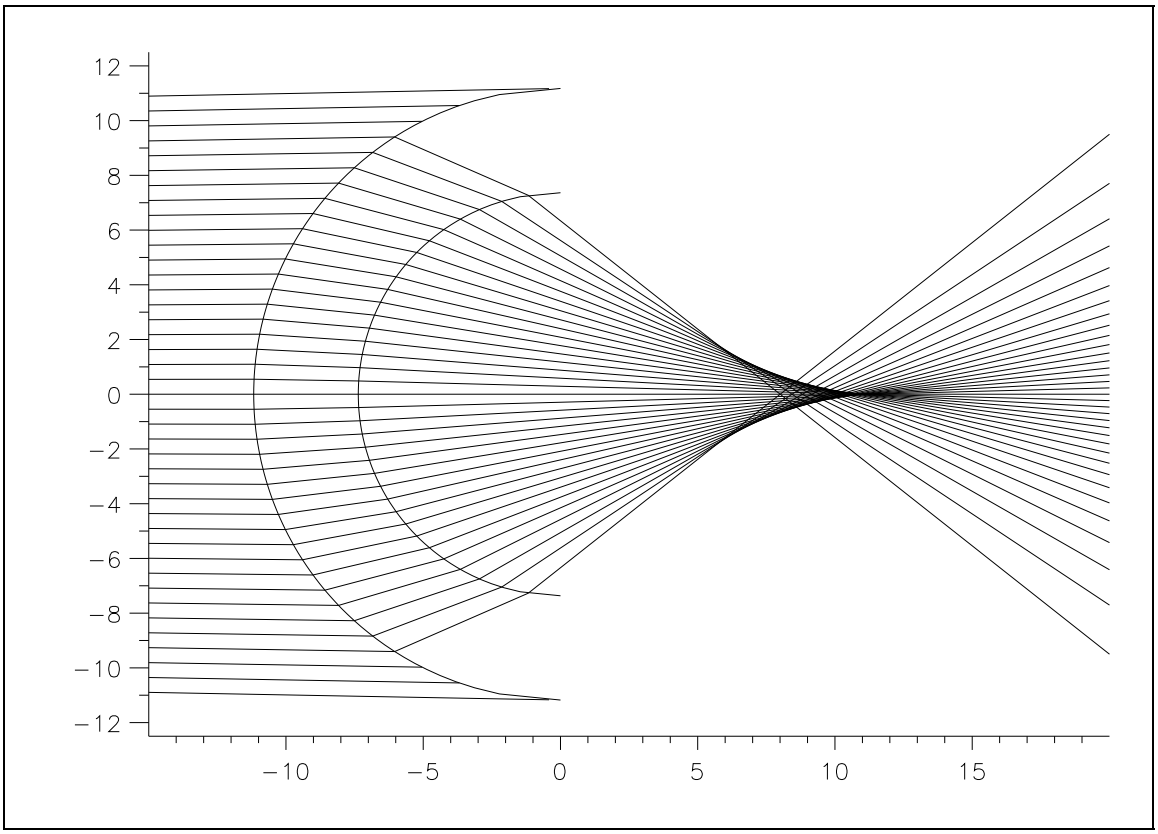

Figure 5.1 - 200 kHz Diver-Held Sonar Lens

23 E.O. Belcher "A Multibeam Diver-Held Sonar With Visual Display," Informal Report, Applied Physics Laboratory, University of Washington, March 1993.

radius 11.176 cm. The speed of sound in the shell is described by the equation 960.6-2.93T m/sec, where T is the ambient temperature in degrees Celsius. The retina radius was fixed at 9.398 cm; and the element was round with diameter 0.3175 cm. The shell could be filled with different mixes of liquids to provide appropriate focus for different temperatures. The parameters for the three trials that were run are tabulated in Table 5.1a.

Table 5.1a - Parameters for 200 kHz Lens

			Sound Speed, m/sec		
Temperature °C	Fluid Mix	Density g/cm^3	Water	Shell	Fluid
21.5	71% FS-5[24], 29% FC-72[25]	1.87	1486.2	897.6	797.7-3.1T (731.1)
13.5	71% FS-5, 29% FC-72	1.87	1459.9	921.0	797.7-3.1T (755.9)
8.0	65% FS-5, 35% FC-72	1.86	1438.6	937.2	776.3-2.94T (752.8)

A comparison of the results from the simulation are compared to the experimental data in Table 5.1b. The focal points shown were found by the simulation; experimentally determined focal points were not available. Two beam patterns were calculated for each trial. The first used the same retina radius (9.398 cm) as the experimental configuration. The second used the focal point which the simulation determined for the retina radius.

24 Occidental Chemical Corp., Fluorolube Lubricant, Grade FS-5

25 3M Fluoroinert Electronic Fluid, Grade FC-72

Table 5.1b - Comparison of Results for 200 kHz Lens

Trial	Retina Radius cm	3 dB Beamwidth degrees	Sidelobe Height dB	Sidelobe Position degrees
1:Experimental	9.398	3°	-19.5, -22	4 to 6°
1:Simulation	9.398	2.9°	-16.7	4.4°
1:Simulation	8.49	2.2°	-16.0	3.5°
2:Experimental	9.398	2.3°	-10 to -12	3 to 4°
2:Simulation	9.398	2.2°	-16.7	3.8°
2:Simulation	9.245	2.2°	-15.6	3.6°
3:Experimental	9.398	2.5°	-15	3°
3:Simulation	9.398	2.2°	-16.5	3.6°
3:Simulation	9.279	2.2°	-15.6	3.5°

The experimental data was taken from printed plots and could only be read to about 0.5° accuracy for the beam widths, 1 dB accuracy for the sidelobe heights, and 1° accuracy for the sidelobe positions. For all three trials, the simulated beam widths were within 0.3° of those experimentally determined and the sidelobe positions were within 1° of those experimentally determined. The sidelobe heights for the first and third trials were within 3 dB of the experimental data, but the second trail was off by between 5 and 7 dB.

The experimental data suggests that the second trial wasn't well focused (resulting in the large sidelobe level) due to using the summer fluid mix at a too-cool temperature of 13.5 °C. The simulation doesn't predict this problem, however.

The simulation predicts nearly identical results for all three trials if the retina radius is set to the focal point instead of being fixed at 9.398 cm. Thus changing the fluid mix and the retina radius can adapt the lens system to a wide temperature range with little or no degradation of performance. It would be interesting to see if this prediction held up in an experimental trial.

5.2 300 kHz Autonomous Underwater Vehicle Lens Analysis

The second lens tested was designed for an autonomous underwater vehicle[26], with 1.5° beams at 300 kHz. Its spherical shell was made of polypropylene with an inner radius of 11.18 cm and an outer radius of 11.89 cm. The retina was fixed at 15.24 cm, and the element used was square with sides 0.3175 cm long. The sound speed in the shell was 2246-2.97T. Two different fluid mixes were used. Mix 1 consisted of 43% DC200-20CS[27], 50% FS-5, and 7% FC-76[28],

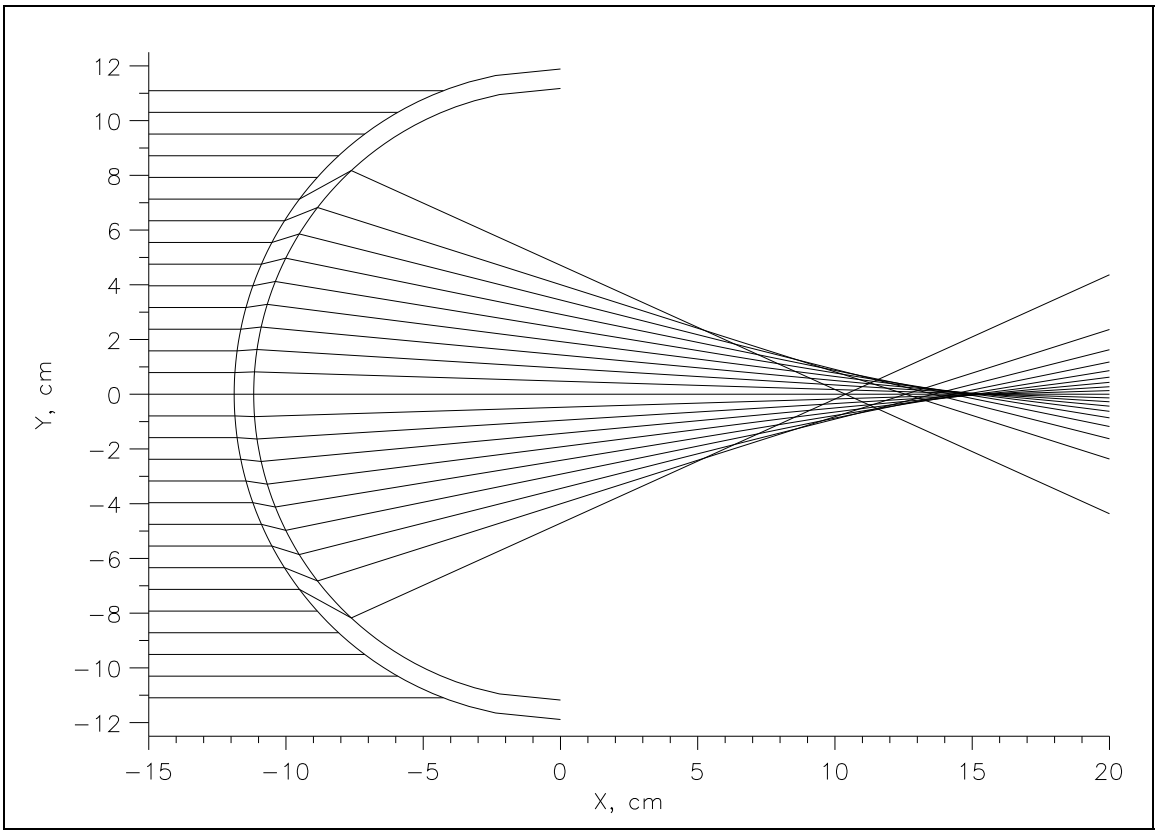

Figure 5.2 - 300 kHz Autonomous Underwater Vehicle Lens

26 E. O. Belcher, D. Steiger, and L. Rosenblum, "A Forward Looking Active Acoustic Lens," Technical Report APL-UW TR9113, Applied Physics Laboratory, University of Washington. May 1991.

27 Dow Corning 200 Fluid, 20 centistoke viscosity

28 3M Fluorinert Electronic Fluid, Grade FC-76

giving a sound speed of 958-3.1T m/sec, where T is the fluid temperature in °C. Mix 2 consisted of 73% DC200, 17% FT (Freon), and 10% FC-72, for a sound speed of 921-3.8T m/sec.

Table 5.2a - Parameters for 300 kHz Lens

Temperature °C	Fluid Mix	Density g/cm^3	Sound Speed, m/sec		
			Water	Shell	Fluid
17.8	Mix 1	1.32	1474.7	2193.1	902.8
12.0	Mix 2	1.8	1454.3	2210.4	875.4
17.0	Mix 2	1.8	1472.0	2195.5	856.4
21.0	Mix 2	1.8	1484.7	2183.6	841.2

Due to the thinness of the shell in this case, the ray tracing procedure may not accurately model the sound propagation. Looking at the ray trace plots, the geometrical acoustics predicts that a large proportion of the lens aperture completely blocks (or reflects) the incident sound. This is almost certainly not the case physically, but the appropriate model is not known at this time.

In order to match the empirical results more closely, trials were run approximating the shell as an infinitely thin interface with radius 11.176 cm (the inner radius of the actual physical shell) and 11.887 cm (the outer radius of the physical shell). It has also been found in previous experiments that using an effective aperture of 80% of the actual lens radius results in closer agreement with experimental results, so that was tried as well. Ray theory predicts that no rays will pass through an interface if they impact it at more than some critical angle. This critical angle prediction is not true in reality, and thus the simulation results in incorrect predictions. The 80% effective aperture represents a compromise between the true thick shell, which can not be modelled by geometric acoustics and a single interface with the same aperture as the thick shell.

In all cases the element was modelled as a square with 0.3175 cm sides, sampled 25 times, with uniform response over the face.

The results from all trials are tabulated below (Tables 5.2b through 5.2e). Note that the focal points for the experimental results are not measured values. They were calculated using the empirically derived thin shell formula[29]

$$\frac{c_0}{c_2} = 0.95\frac{(r+R)}{R} \quad ,$$

where c_0 is the speed of sound in water,

c_2 is the speed of sound in the lens fluid,

r is the inside radius of the shell, and

R is the focal distance, measured from the center of the lens.

Table 5.2b - 300 kHz AUV @ 17.8° C

Trial	Focal Point, cm	Beam Width, degrees	Sidelobe Height, dB	Sidelobe Position, degrees
Experimental	15.5	1.5	-16	2
Full Shell	13.7	2.2	-21.2	3.5
Inner Shell	14.6	1.6	-16.6	2.7
Outer Shell	15.6	1.4	-11.1	2.1
Inner Shell, 80% Aperture	15.5	1.6	-16.9	2.6
Outer Shell, 80% Aperture	16.5	1.5	-10.3	2.1

29 E. O. Belcher, C. May, and E. Pence, "Active Acoustic Lens with Large Field of View, Final Report," Technical Report APL-UW TR8918, Applied Physics Laboratory, University of Washington. June 1989. pg. 22.

Table 5.2c - 300 kHz AUV @ 12° C

Trial	Focal Point, cm	Beam Width, degrees	Sidelobe Height, dB	Sidelobe Position, degrees
Experimental	14.9	1.5	-11 to -15	1.5 to 2
Full Shell	13.3	2.1	-20.9	3.6
Inner Shell	14.1	1.7	-17.6	2.9
Outer Shell	15.0	1.4	-14.7	2.3
Inner Shell, 80% Aperture	14.9	1.6	-20.1	2.7
Outer Shell, 80% Aperture	15.8	1.5	-14.3	2.3

Table 5.2d - 300 kHz AUV @ 17° C

Trial	Focal Point, cm	Beam Width, degrees	Sidelobe Height, dB	Sidelobe Position, degrees
Experimental	13.8	2	-19.5	4 to 6
Full Shell	12.3	2.3	-20.5	5.0
Inner Shell	13.1	2.0	-17.0	3.6
Outer Shell	13.9	1.6	-18.0	2.8
Inner Shell, 80% Aperture	13.7	1.7	-20.0	3.5
Outer Shell, 80% Aperture	14.6	1.5	-21.2	2.6

Table 5.2e - 300 kHz AUV @ 21° C

Trial	Focal Point, cm	Beam Width, degrees	Sidelobe Height, dB	Sidelobe Position, degrees
Experimental	13.0	2	-16 to -19	7 to 9
Full Shell	11.7	2.7	-17.8	5.1
Inner Shell	12.3	2.6	-17.1	4.8
Outer Shell	13.2	2.0	-16.5	3.3
Inner Shell, 80% Aperture	13.0	2.3	-14.5,-18.9	3.5,4.9
Outer Shell, 80% Aperture	13.8	1.7	-19.5	3.3

The simulations using the shell material showed larger beam widths, lower sidelobes, and closer focal distances than the experimental data. The zero-thickness shell simulations' predictions were closer to matching. The simulations using the outer shell and the inner shell with 80% aperture were the closest in all cases to the experimental data. The inner shell 80% aperture focal distances were identical to those predicted by the thin shell formula, and the beam widths were all within 0.5°, which is as accurately as the experimental data can be read. The simulated sidelobes tended to be lower and positioned farther away from the main lobe than they were in the experimental data, but were not dramatically different in any case.

5.3 100 kHz Underwater Surveillance Sonar Lens Analysis

Beam patterns for several retina positions for five different fluid/temperature configurations for a thick lens designed for an underwater surveillance sonar system were also available[30]. The lens used was similar to the 300 kHz lens, but used a 12.7 cm, 0.3175 cm thick ABS shell and operated at 100 kHz (Figure 5.3a). Table 5.3a shows the parameters for the five trials performed.

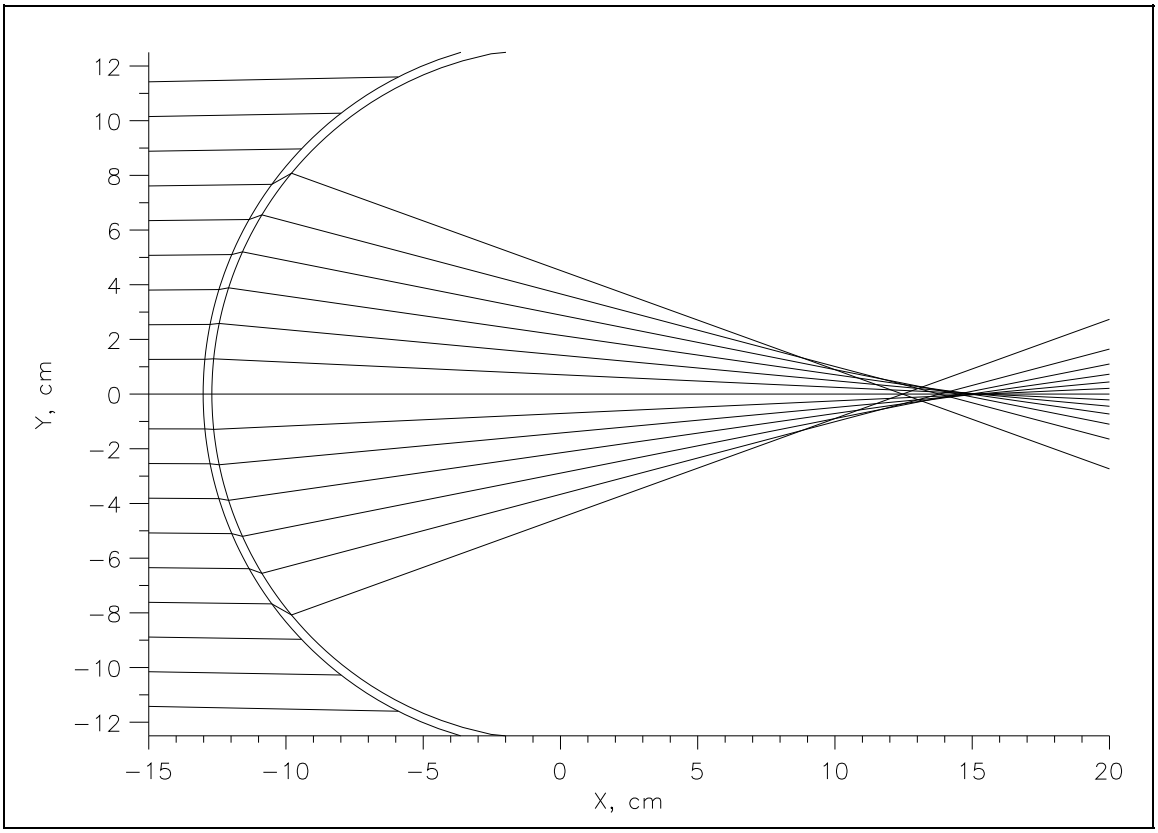

Figure 5.3a - 100 kHz Surveillance Sonar Lens

30 E. O. Belcher and W. H. Hanot, "Acoustic Lens Sensor Designs for a Surveillance Sonar," Technical Report APL-UW TR9214, Applied Physics Laboratory, University of Washington. October 1992.

Table 5.3 - Parameters for 100 kHz Lens

Trial	Temperature °C	Fluid Mix	Fluid Speed m/sec	Fluid Density g/cm^3	TR9214 Figure
a	6.1	71% FS5, 29% FC72	797.7-3.1T	1.87	5.7
b	11.8	89% FS5, 11% FC77	893.4-3.1T	1.91	5.6
c	18.7	72% FS5, 28% FC77	844.0-3.1T	1.89	5.10
d	20.0	52% FS5, 48% FC101	820.7-3.0T	1.856	5.9
e	22.0	89% FS5, 11% FC77	893.4-3.1T	1.91	5.8

The simulations using the full shell did not agree well with the experimental data (Figures 5.3b and 5.3c, for example). The ray trace plot (Figure 5.3a) shows that the lens shell causes many of the rays to be discarded due to exceeding the critical angle condition. The critical angle condition is a prediction of geometric acoustics but not wave acoustics and thus is not accurate in all cases.

In order to better match the experimental results, the lens shell was modelled as an infinitely thin interface with radius equal to the inner radius of the physical shell. Simulations were run with lens apertures of 100%, 90%, and 80% of the physical aperture to approximate the shading of the true shell. These simulations matched the experimental results much better. In general, the 100% aperture simulations predicted a focal point just inside of the experimentally determined focal point and a smaller focal depth than the experimental data suggested. The simulated focal point moved out and the focal depth increased with decreasing aperture size. The 90% aperture trials seemed to match the experimental data most closely (Figures 5.3b and 5.3c). For some trials, though, the focal point was shifted by up to 1 cm (Figure 5.3c). The reasons for this have not yet been determined.

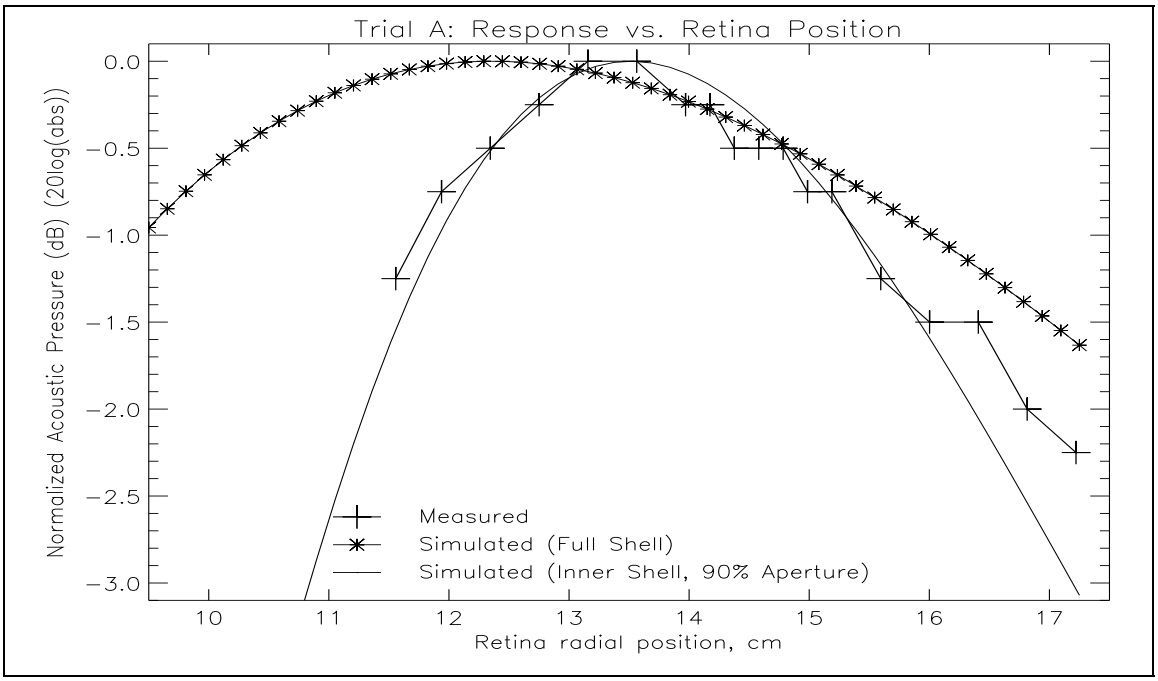

Figure 5.3b - Trial A: Focal Depth Results

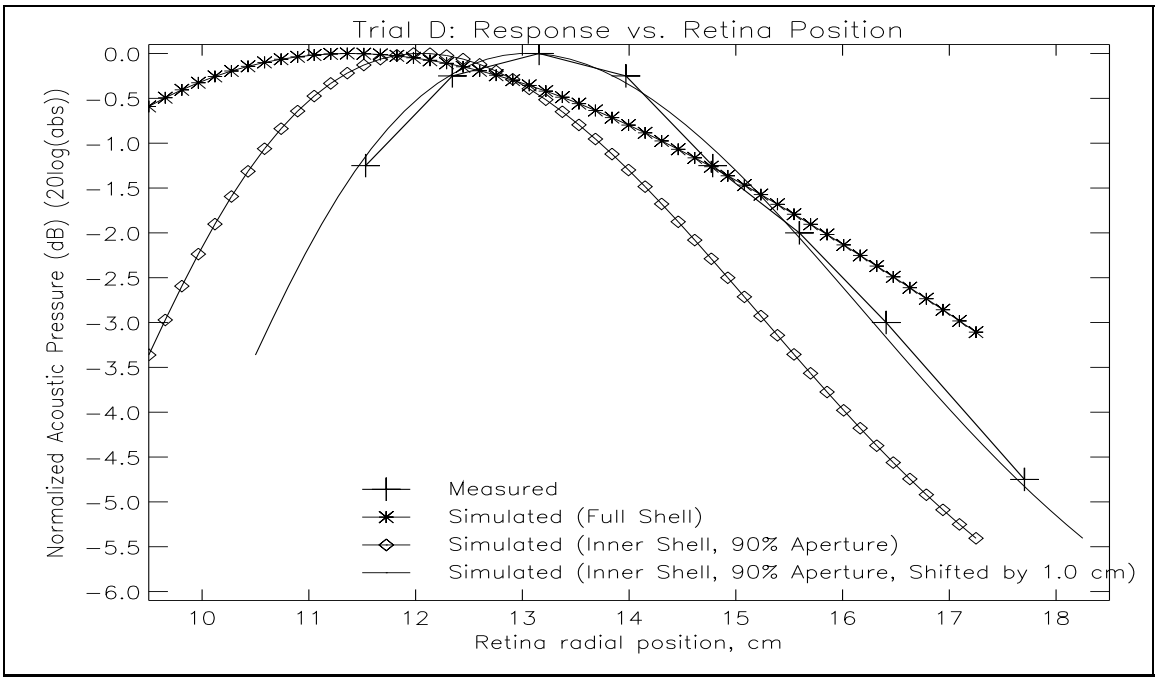

Figure 5.3c - Trial D: Focal Depth Results

5.4 Effect of Varying System Parameters on Pressure Fields

Many of the system parameters cause definite, repeatable changes in the pressure fields and beam patterns of lens systems. For example, if a lens system is to be used at several temperatures, it is useful to know how its performance will be affected by varying temperature. ALSSP is useful in investigating these effects.

5.4.1 Water Temperature

Increasing the ambient water temperature moves the focal point of a lens system in and decreases the depth of focus. Figure 5.4.1a is a contour plot of the pressure field behind the lens described in section 5.3. The lens was simulated using the full shell, the operating frequency was set to 100 kHz, and the ambient water temperature was 6.1 °C.

After changing the ambient water temperature to 20 °C (Figure 5.4.1b), the focal point shifted from 12.2 cm to 10.8 cm (a -12% change), and the depth of focus (distance between the 3 dB points in the radial direction) decreased from 11.4 cm to 8.4 cm (a -26% change). The change in the focal point is much less than the focal depth at either temperature, so a retina position could easily be chosen that would provide good results at either temperature. In fact, the compromise retina position of 11.4 cm is only 0.1 dB down from the peaks of the two focal points.

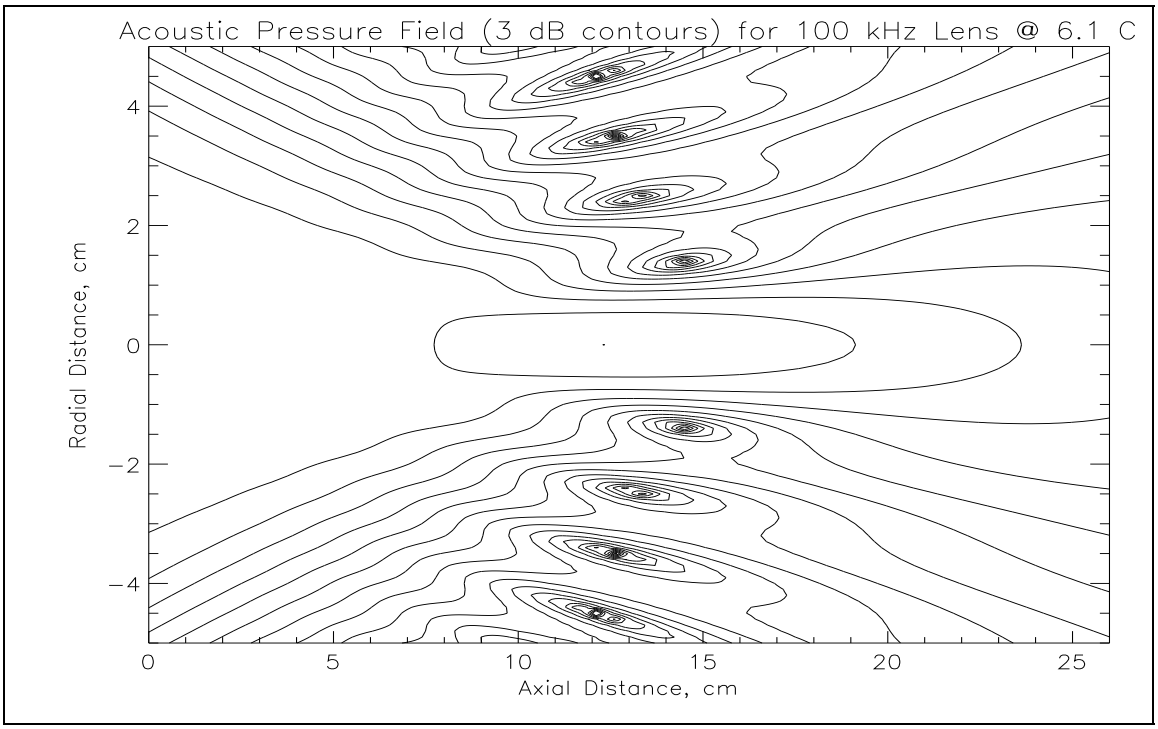

Figure 5.4.1a - 3 dB Contour Plot of Trial A: 100 kHz, 6.1 °C

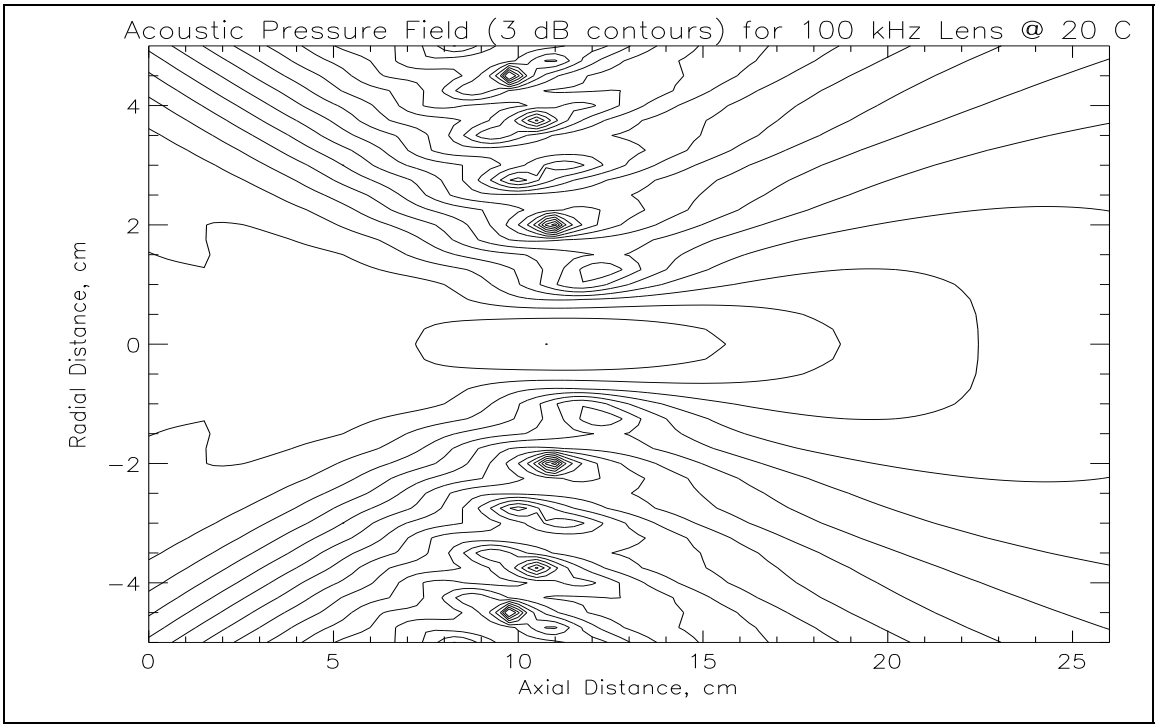

Figure 5.4.1b - 3 dB Contour Plot of Trial A: 100 kHz, 20 °C

5.4.2 Frequency

Increasing the operating frequency of a lens system changes the pressure field drastically. The entire field appears to be compressed and shifted out at higher frequencies. This moves the focal point out and decreases the focal depth. In terms of beam patterns, the beam width decreases with increasing operating frequency and the sidelobes move in. Sidelobe heights aren't greatly affected, but do tend to decrease slightly. To a first approximation, the pressure field is scaled by the frequency, so changing from 100 kHz to 300 kHz will compress the pressure field by a factor of 3.

Figure 5.4.2a shows the pressure field of the same lens as Figure 5.4.1a, but operating at 300 kHz instead of 100 kHz. The focal point moved from 12.2 cm to 13.9 cm (a 14% change), and the depth of focus decreased from 11.4 cm to 4.5 cm (a -61% change).

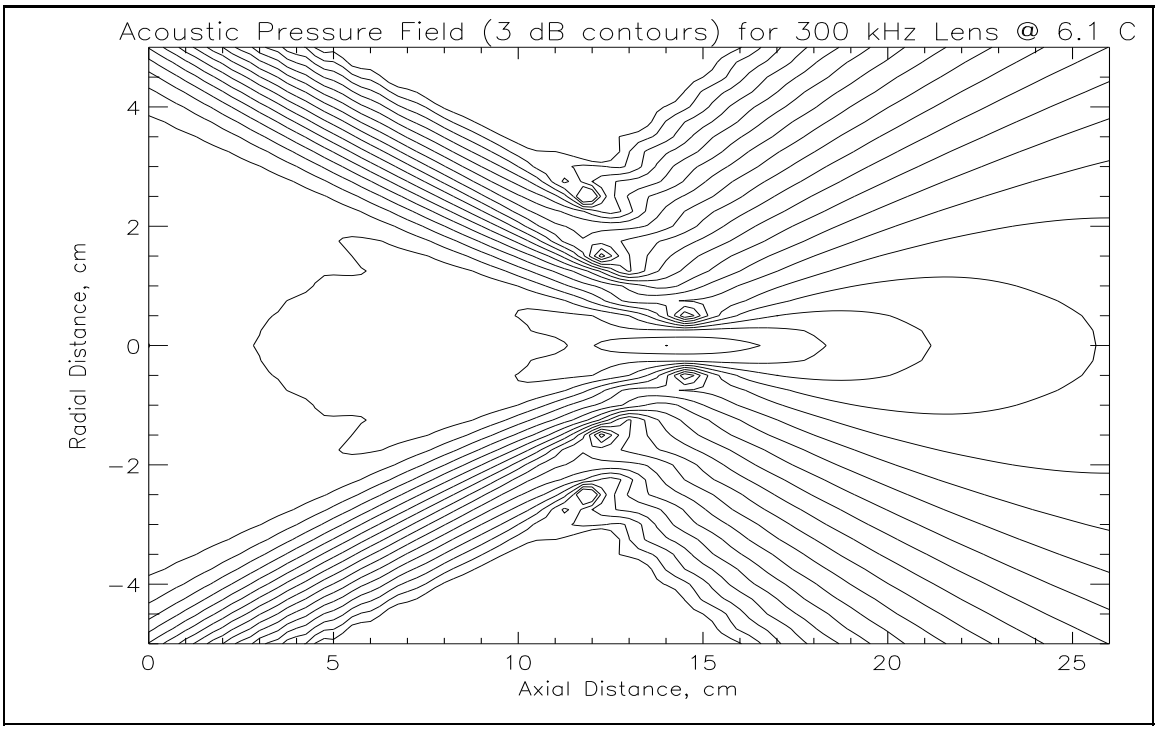

Figure 5.4.2a - 3 dB Contour Plot of Trial A: 300 kHz, 6.1 °C

Figure 5.4.2b shows beam patterns for the system operating at 6.1 °C for the two operating frequencies. The retina radius was set to the focal point of system in each case. The beam width decreased from 5.1° to 1.6° (a -69% change) and the sidelobe heights decreased slightly, from -13.5 dB to -14.1 dB (a -4% change).

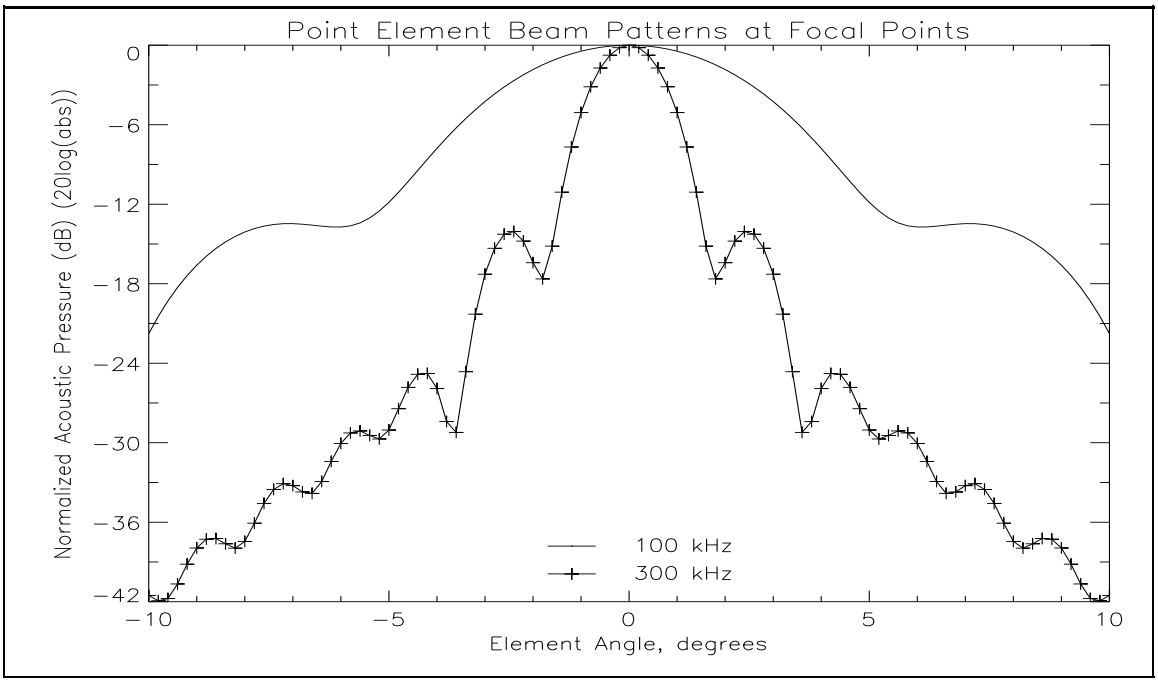

Figure 5.4.2b - Effect of Frequency on Beam Patterns

The effects of changing temperature are more drastic at higher frequencies because the pressure field is compressed. Figure 5.4.2c shows the pressure field for the lens operating at 300 kHz and 20 °C. The focal point moved in from 13.9 cm to 11.6 cm (-17%) and the focal depth decreased from 4.5 cm to 3.2 cm (-29%). The compromise retina position of 12.7 cm is 1.2 dB down from the peaks rather than the 0.1 dB of the 100 kHz system. The 300 kHz lens system will thus be much more sensitive to water temperature than the 100 kHz system.

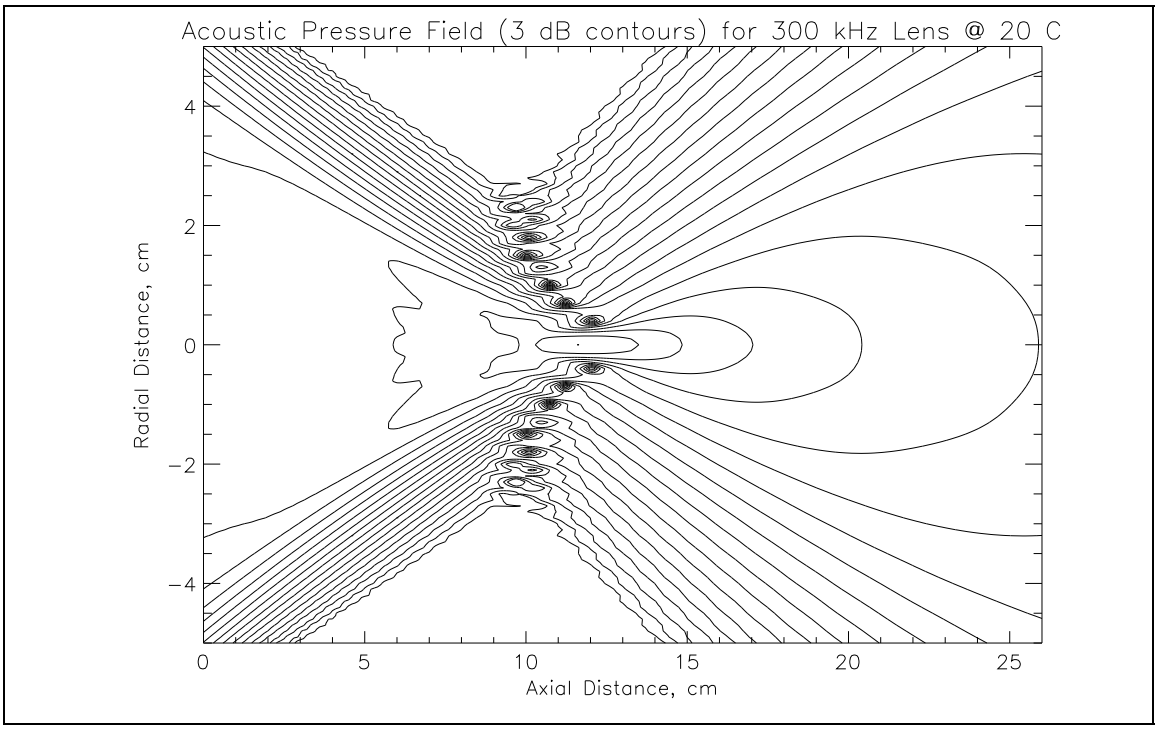

Figure 5.4.2c - 3 dB Contour Plot of Trial A: 300 kHz, 20 °C

5.4.3 Element Size

Introducing an element into a pressure field is equivalent to performing a convolution of the pressure field with an element function. For a point element, the pressure field is convolved with an impulse function, and thus is not changed. Therefore, the position of maximum response of a point element is the focal point of the lens system. For a larger element, however, the element function has larger support and the pressure field is "smoothed". Because of this, the position at which the element responds most strongly to the pressure field (the apparent focal point) will not be at the system's focal point. Increasing the element size moves the apparent focal point out and increases the apparent depth of focus. Figure 5.4.3a compares the response of a point element, a 1.0 cm diameter element, and a 2.0 cm diameter element moving along the x-axis of a lens system.

Increasing the element size also increases the beam width and decreases the sidelobe heights of beam patterns. Figure 5.4.3b compares the beam patterns of lens system using a point element, a 1.0 cm diameter element, and a 2.0 cm diameter

element. The beam width increases from 3.1° to 3.4° to 5.0° and the sidelobes drop from -10.8 dB to -11.7 dB to about -17 dB.

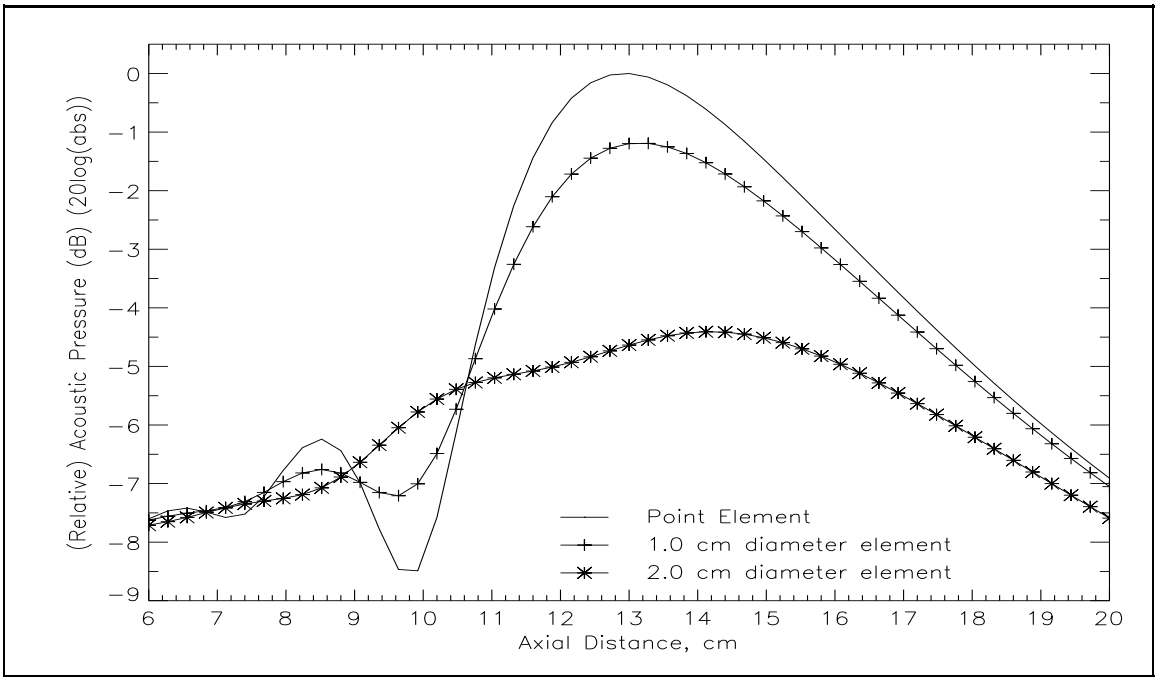

Figure 5.4.3a - Effect of Element Size on Axial Response

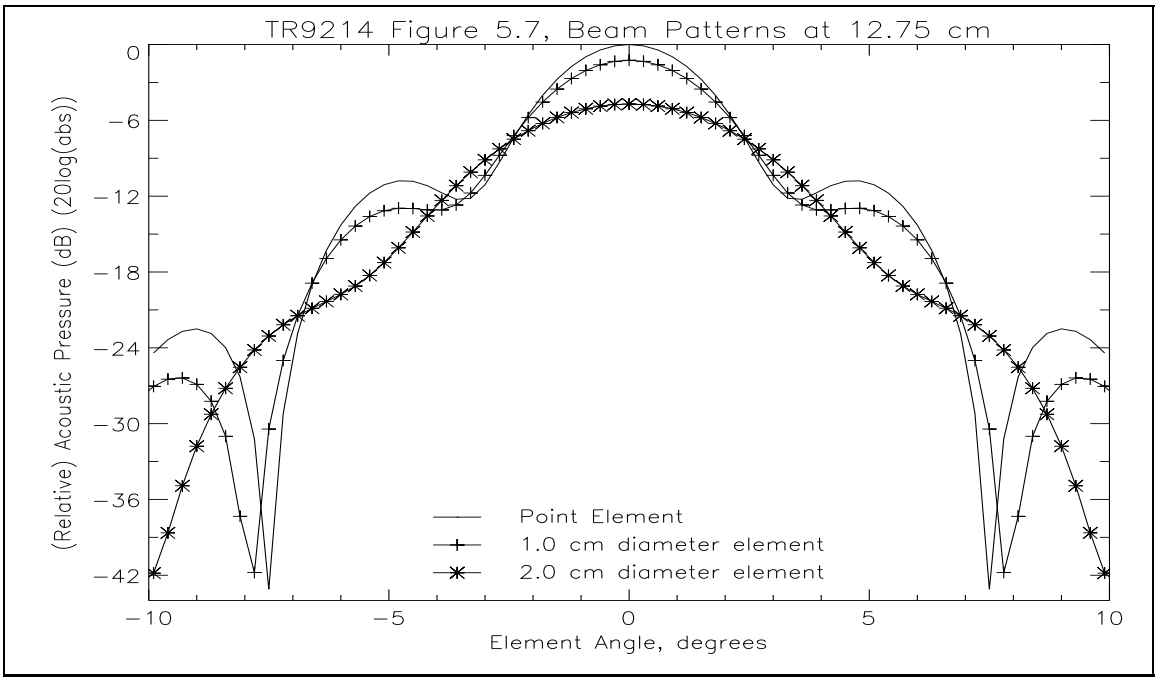

Figure 5.4.3b - Effect of Element Size on Beam Patterns

5.4.4 Shading Due to Sound Attenuation in Lens Material

Sound attenuation in the lens material has the effect of "shading" the aperture. Lens materials often have much higher sound attenuation rates than the surrounding water or the lens fluid. In addition, rays farther from the lens center travel a longer distance through the lens material than those close to the center, and thus are attenuated even more. The magnitude of sound coming from the edges of the lens, then, is less than that from the center. This has the effect of moving the focal point out from the lens system and increasing the depth of focus. It also widens beam patterns, increasing the beam width and moving the sidelobes out. The height of the sidelobes is also reduced. Table 5.4.4a shows parameters for the 200 kHz lens described in section 5.1 with no attenuation in the shell material, 1.0 dB/cm attenuation, 2.5 dB/cm attenuation, 5.0 dB/cm attenuation, and 10.0 dB/cm attenuation. The focal point isn't greatly affected, but the depth of focus and beamwidths are strong functions of the attenuation rate.

The actual attenuation rate in the shell material for the 200 kHz lens is not known. However, similar materials have attenuation rates in the vicinity of 2 to 6 dB/cm. The response of the lens with 10 dB/cm attenuation is 40 dB lower than that with no attenuation, which would result in undetectable signal levels. Since the lens did in fact focus sound into detectable levels, the attenuation rate must have been much smaller than 10 dB/cm.

Table 5.4.4a - Thick Lens Parameters as Function of Material Attenuation Rate

Attenuation Rate, dB/cm	Focal Point, cm	Focal Depth, cm	Beam Width, degrees	Sidelobe Height, dB
0.0	10.3	2.6	1.9	-10.4
1.0	10.3	2.7	2.0	-10.8
2.5	10.4	2.9	2.1	-11.4
5.0	10.4	3.3	2.2	-13.1
10.0	10.5	3.9	2.5	-14.1

The effect of attenuation in the lens material is much more pronounced in the case of thin lenses, since they are generally thicker near the edges than near the center. Table 5.4.4b shows that changing the attenuation rate from 0.0 to 2.5 dB/cm for a thin lens changes the beam width by 14% and the sidelobe height by 33%, whereas the respective changes were only 11% and 10% for the same attenuation rates in the thick lens. The focal depth changed by about the same percentage (10%) in both the thick and thin lens cases.

Table 5.4.4b - Thin Lens Parameters as Function of Material Attenuation Rate

Attenuation Rate, dB/cm	Focal Point, cm	Focal Depth, cm	Beam Width, degrees	Sidelobe Height, dB
0.0	7.622	1.976	0.138	-8.2
2.5	7.663	2.202	0.158	-10.9

5.4.5 Aperture Size

Incorporating sound attenuation is theoretically sound, but requires knowledge of the sound attenuation rate in each material. This is generally a function of frequency and temperature, and may not be readily available. In addition, for thick lenses, incorporating sound attenuation requires the use of a shell. In some cases that may cause problems (see section 5.3), so an alternate method is used.

Decreasing the aperture size of a lens system is one way to approximate the attenuation of the lens material without requiring a shell and knowledge of the sound attenuation rate in the shell. It is equivalent to making the attenuation rate infinite beyond a certain radius of the lens, while not changing it within that radius. Reducing the aperture of a lens system often helps make a simulation agree with experimental results, but doesn't have as strong a justification as incorporating the attenuation rate of the lens material.

Decreasing the aperture moves the focal point out, increases the depth of focus, widens beam patterns and modifies sidelobe heights and positions. Since sidelobes are effects of interference between the virtual point sources on the final lens surface, the

change in their heights doesn't follow a simple rule. Table 5.4.5a shows the parameters of the 200 kHz lens system described in section 5.1 at 100%, 90%, and 80% of full aperture. Figure 5.4.5 shows beam patterns for the same system.

Table 5.4.5 - Thick Lens Parameters as Function of Aperture Size

Aperture Size, Percent of Full	Focal Point, cm	Focal Depth, cm	Beam Width, degrees	Sidelobe Height, dB
100	10.3	2.6	1.9	-10.4
90	10.8	3.8	2.3	-13.0
80	10.8	5.3	2.7	-12.8

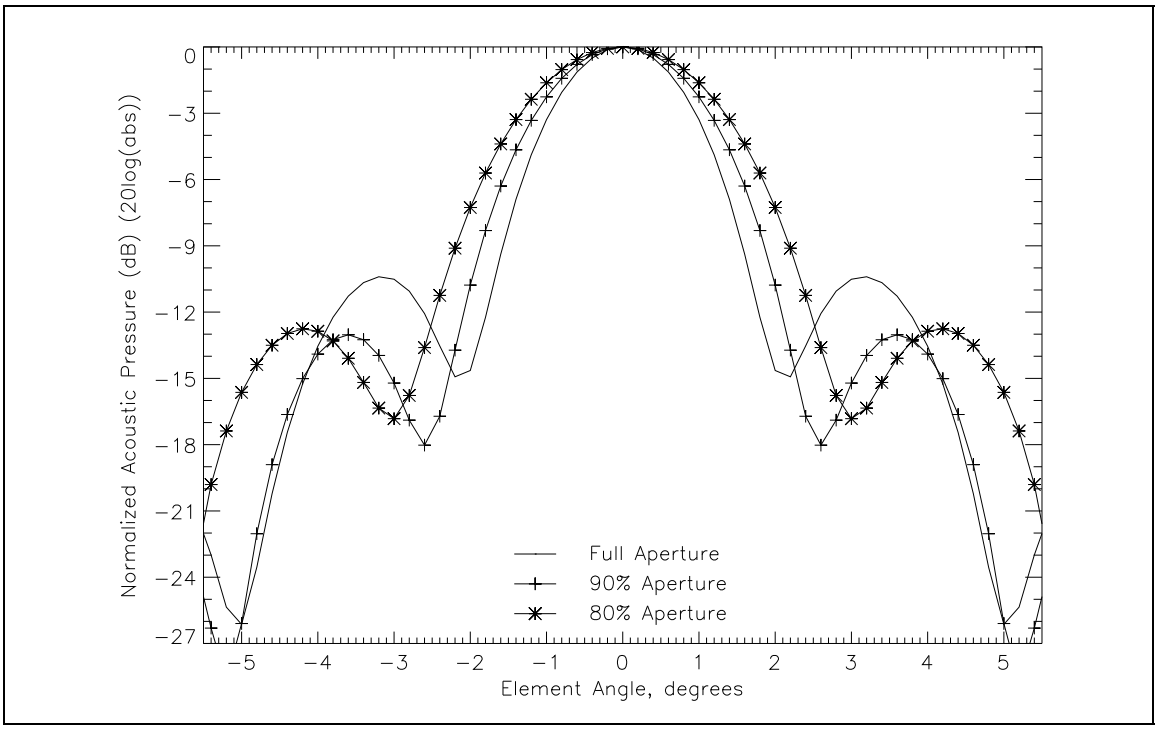

Figure 5.4.5 - Effect of Aperture Size on Beam Patterns

5.5 Thin Lens Design

To illustrate the use of ALSSP in an iterative design project, a thin lens system has been designed that is to operate at 900 kHz in 10 °C fresh water. The beams formed should be less than 0.25° wide with sidelobes more than 40 dB down within a 10° field of view, and less than 0.5° wide with sidelobes more than 20 dB down within a 50° field of view. The element size and positioning need to be determined in order to finish the system design. For a more complete explanation of the commands required to execute this example, see the ALSSP User's Manual.

The first step in setting up a lens system is to build the system parameter file. This lens system was designed using BEAM THREE, so the OPTICS file, which contains the lens interface and material information, is available.

GENERATE_SYSTEM will convert the OPTICS file to a form that CALC_LENS can use. However, BEAM THREE only does ray tracing, so does not provide information about the system frequency or the ambient conditions. The frequency (900 kHz), water salinity (0 parts per thousand), water depth (1.0 meter), water density (1.0 g/cm^3), rate of sound attenuation in water (0.0 dB/cm), and the number of rays to trace (301) will be stored in a system header file 'system_header'.

In order to decide where elements should be placed, the focal point of the system for various source angles must be found. GENERATE_SYSTEM will make parameter files to do this automatically if given the desired source angles. Source angles of 0°, 1°, 2.5°, 5°, 10°, and 25° will provide a good picture of the retina shape. In addition, the point source distance must be defined. For this lens system, the targets will be approximately 25 meters from the lens, so the point source will be positioned 25 meters from the first lens surface. The lens material used is syntactic foam, which has a sound attenuation rate of approximately 1.0 dB/cm at 900 kHz.

In Figure 5.5a, the lens system is the five curved surfaces on the left and the retina is the plus symbols connected by line segments. The left-most lens element is an iris, implemented as a planar surface that doesn't affect the rays except to define the aperture of the system. The iris could be eliminated by setting the first lens interface's aperture to the diameter of the iris, but GENERATE_SYSTEM takes the

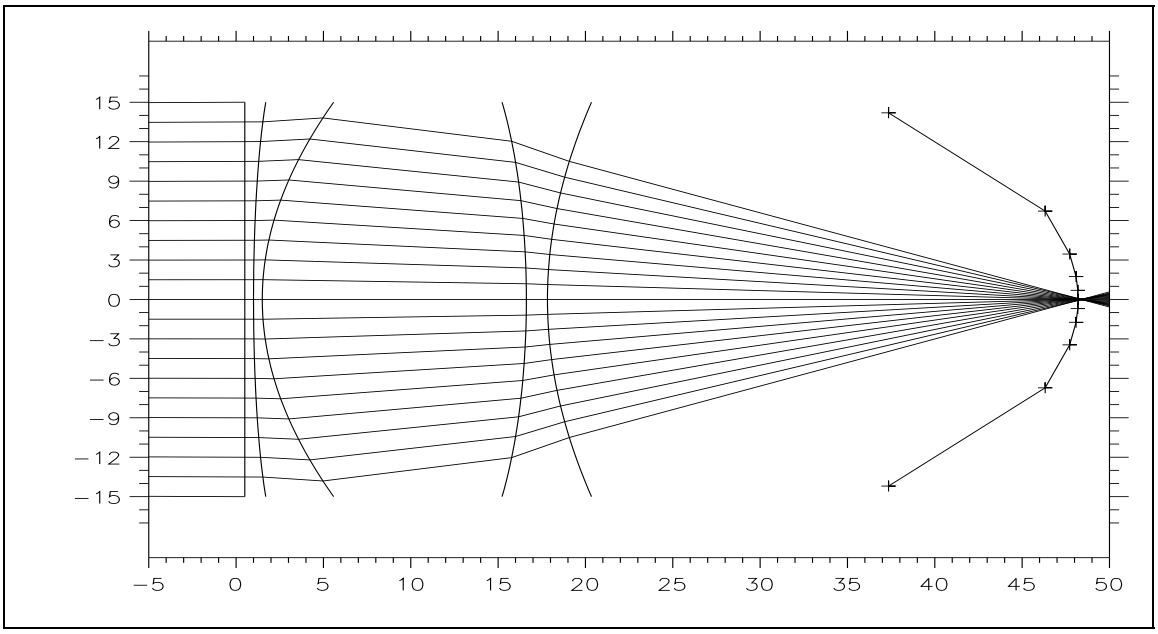

Figure 5.5a - Thin Lens System with Focal Trajectory

interfaces directly from the OPTICS file, so it is included as a separate element.

The next two surfaces represent the first syntactic foam lens. The first is an oblate ellipsoid, the second a hyperboloid. The final two surfaces are a second syntactic foam lens. The front surface is another hyperboloid and the back surface is a prolate ellipsoid.

The focal points found for each source angle are shown as plus symbols ('+') in the figure, and are joined by line segments to approximate the ideal retina shape for the lens system. Note that this system is symmetric about the x-axis, so the focal points found for positive source angles can be mirrored for the corresponding negative source angles.

The next step in analyzing the system is to compute beam patterns. The program MAKE_BEAMS2 will be used to generate the parameter files to do this. Since the retina is not an arc, the element must be moved along a trajectory approximating the retina shape. However, the retina can be approximated as a collection of arcs for small changes in the source angle. The center of each arc is referred to as the secondary principal point in optical lens design. The program FOCI_CIRC1 finds the parameters of these arcs.

Representative two way beam patterns (the complex pressure is squared in order to simulate a lens system used for both transmitting and receiving) are shown in Figures 5.5b and 5.5c. The numerical results are tabulated in Table 5.5a.

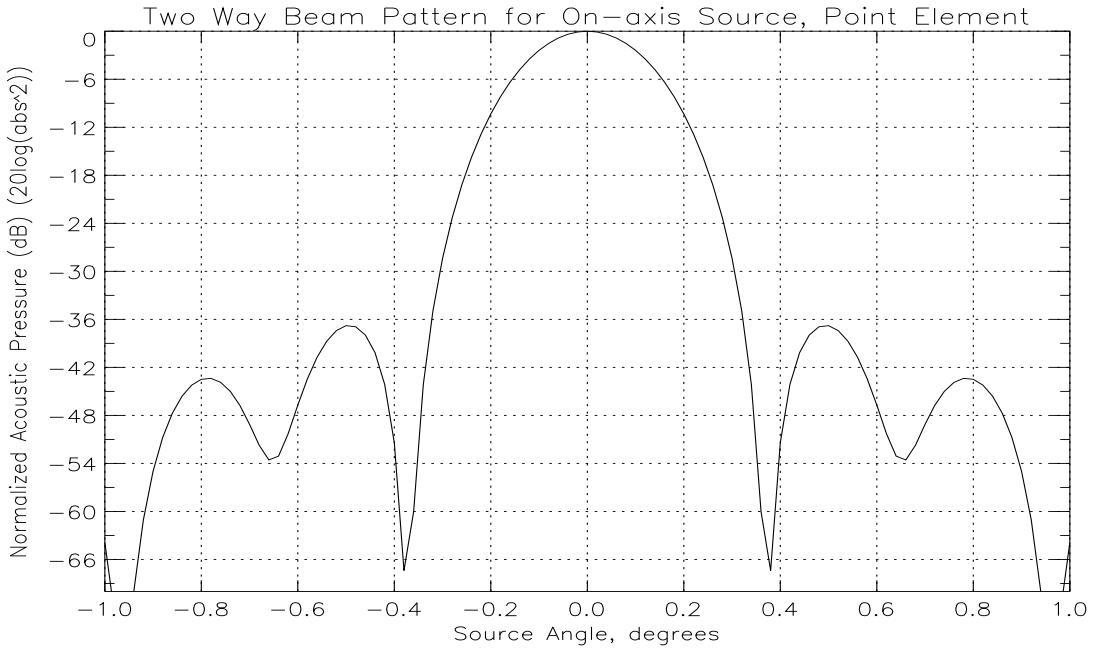

Figure 5.5b - Beam Pattern for On-Axis Point Source

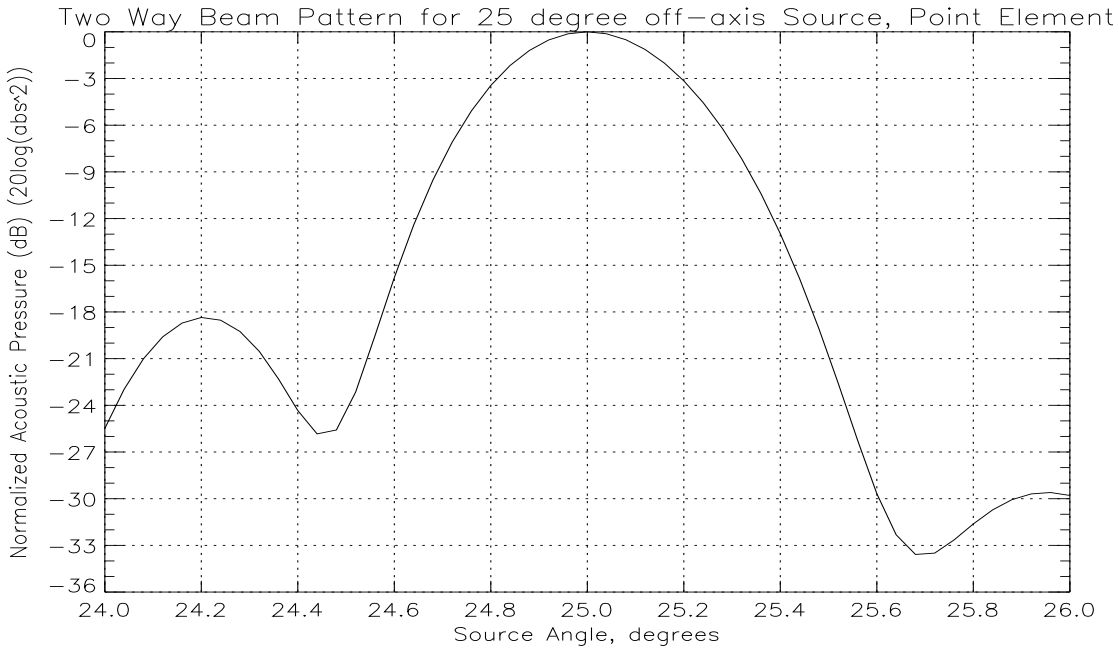

Figure 5.5c - Beam Pattern for 25° Off-Axis Point Source

Table 5.5a - Point Element Data for Thin Lens System		
Source Location	Two-way beam width	Sidelobe Level
0°	0.223°	-36.8 dB
5°	0.224°	-34.8 dB
10°	0.232°	-32.6 dB
25°	0.377°	-18.4 dB

Table 5.5a shows the beam widths are all within the specifications, but the sidelobe levels are all too high. However, these calculations were made for a point element. Any real element will have a physical size and shape that will affect the beam widths and sidelobe levels. By adding the effect of element size and shape into the calculations, the sidelobe levels can be decreased for a small penalty in beam width. For example, adding a 0.268 cm element results in similar beam patterns, but ones that exhibit slightly larger beam widths and lower sidelobe levels, as expected. The results are tabulated in Table 5.5b:

Table 5.5b - 0.268 cm Element Data for Thin Lens System		
Source Location	Two-way beam width	Sidelobe Level
0°	0.246°	-47.8 dB
5°	0.248°	-46.8 dB
10°	0.255°	-44.6 dB
25°	0.401°	-22.6 dB

Now the specifications have been met. For the 10° field of view, the beam widths are under 0.25° and the sidelobe levels are below -40 dB. For the 50° field of view, the beam widths are under 0.5° and the sidelobe levels are below -20 dB.

Chapter 6: CONCLUSION

The Acoustic Lens Simulation Software Package (ALSSP) was developed to analyze acoustic lens systems and predict the performance of a lens design before fabrication. Given a design, the simulation determines the beam pattern as a function of temperature, frequency, source position, and the transducer element. ALSSP is useful in the design of lens systems which must operate at multiple temperatures and/or frequencies. In addition, the lens system may consist of an arbitrary number of components of various types and so ALSSP is not limited to analyzing one type of lens system, such as spherical fluid-filled lenses.

The simulation software successfully modelled the general behavior of a variety of spherical, liquid-filled acoustic lenses. It was able to predict beam widths and sidelobe heights and positions for various fluid mixes and shell configurations at different temperatures. For thick lenses with thin-walled shells, better results were obtained from using zero-thickness shells with smaller effective than physical apertures. The simulations were also able to predict depth of focus and approximate focal position with this modification.

The primary limitation of the software seems to be the modelling of the propagation of sound through a thin spherical shell. The present model utilizes the solution of the wave equation for a planar interface to calculate transmission coefficients at each side of the shell. This is done by making the assumption that the shell curvature is small compared to the wavelength of sound. The simulation also ignores the components of rays reflected within the lens system, which may reduce its accuracy for some shell configurations.

ALSSP is also able to model thin lenses. Although experimental data on which to test it is still limited, there is no reason to believe that it should not make accurate predictions. As discussed earlier, other researchers have successfully modeled specific thin lenses using similar algorithms. ALSSP extends those algorithms to a more general class of lenses and environment conditions.

Bibliography

"Beam Three Optical Ray Tracer", Stellar Software, Berkeley, CA.

"PV-WAVE: Workstation Analysis and Visualization Environment," Precision Visuals, Inc., Boulder, CO. Copyright 1990.

W. L. Beaver, D. H. Dameron, and A. Macovski, "Ultrasonic Imaging with an Acoustic Lens," IEEE Transactions on Sonics and Ultrasonics, Vol. SU-24, No. 4, July 1977.

E. O. Belcher, "A Multibeam, Diver-Held Sonar Using a Liquid-Filled, Spherical Acoustic Lens," Proceedings of the Oceans '93 Conference, October, 1993.

E. Belcher, D. Folds, B. Johnson, B. Kamgar-Parsi, and D. Scroggins, "3-D Acoustic Imaging with a Thin Lens," Proceedings of the Oceans '93 Conference, October, 1993.

E. O. Belcher "A Multibeam Diver-Held Sonar With Visual Display," Informal Report, Applied Physics Laboratory, University of Washington, March 1993.

E. O. Belcher and W. H. Hanot, "Acoustic Lens Sensor Designs for a Surveillance Sonar," Technical Report APL-UW TR9214, Applied Physics Laboratory, University of Washington. October 1992.

E. O. Belcher, D. Steiger, and L. Rosenblum, "A Forward Looking Active Acoustic Lens," Technical Report APL-UW TR9113, Applied Physics Laboratory, University of Washington. May 1991.

E. O. Belcher, C. May, and E. Pence, "Active Acoustic Lens with Large Field of View, Final Report," Technical Report APL-UW TR8918, Applied Physics Laboratory, University of Washington. June 1989.

C. S. Clay and H. Medwin, Acoustical Oceanography: Principles and Applications. John Wiley & Sons, 1977.

T. A. Cornelius and K. L. Williams, "Note on the Calculation of the Spherically Aberrated Field of an Acoustic Lens," Technical Memorandum APL-UW TM 7-92, Applied Physics Laboratory, University of Washington, 1992.

D. L. Folds, "Status of Ultrasonic Lens Development," Underwater Acoustics and Signal Processing, pp. 263-279, D. Reidel Publishing Company, 1981.

D. L. Folds, "Focusing properties of a solid four-element ultrasonic lens," The Journal of the Acoustical Society of America, Vol. 58 No. 1, July 1975. pg. 74.

D. L. Folds, "Focusing properties of solid ultrasonic cylindrical lenses," The Journal of the Acoustical Society of America, Vol 53 No 3, 1973. pp 830-831.

D. L. Folds, "Focusing Properties of a Cylindrical Liquid-Filled Compound Acoustic Lens," The Journal of the Acoustical Society of America, Vol. 49 No. 5 (Part 2), 1971.

D. L. Folds and D. H. Brown, "Focusing Properties of Cylindrical Liquid-Filled Acoustic Lenses with Large Diameter-to-Wavelength Ratios," The Journal of the Acoustical Society of America, Vol. 43 No. 3, 1968.

E. Hecht, Optics, Addison-Wesley Publishing Company, 2nd Ed., 1990. pg. 459-463.

N. N. Makarchenko, F. V. Rozhin, and O. S. Tonakanov, "On Choosing the Optimal Parameters of a Spherical Lens," Vestnik Moskovskogo Universiteta, Seriya 3 (Fizika Astronomiya). Vol.44 No. 5, pp. 32-6. 1989.

J. T. Oh and S. B. Park, "Iterative design of a lensed transducer-reflector system for underwater acoustic imaging," The Journal of the Acoustical Society of America, Vol. 93, No. 2, pp. 1166-1174. February 1993.

J. T. Oh and S. B. Park, "Optimal Design of a Transmit/Receive System with a Reflector and a Transducer Lens for Long-Range Underwater Acoustic Imaging," IEEE 1991 Ultrasonics Symposium Proceedings, Vol 2, pp. 949-52. 1991.

A. Penttinen and M. Luukkala, "Sound pressure near the focal area of an ultrasonic lens," Journal of Physics D: Applied Physics, Vol. 9, pp. 1927-36. 1976.

J. T. Shaw, "Tables of Sound Absorption in Sea Water," Technical Note 1-77, Applied Physics Laboratory, University of Washington. October 1976.